

Pathways of Nordic Overflows from climate model scale and eddy resolving simulations

Yeon S. Chang^{a,*}, Zulema D. Garraffo^b, Hartmut Peters^c, Tamay M. Özgökmen^a

^a Rosenstiel School of Marine and Atmospheric Science, University of Miami, 4600 Rickenbacker Causeway, Miami, FL 33149, USA

^b Center for Computational Science, University of Miami, 4600 Rickenbacker Causeway, Miami, FL 33149, USA

^c Earth and Space Research, 2101 Fourth Ave., Seattle, WA 98121, USA

ARTICLE INFO

Article history:

Received 10 October 2008

Received in revised form 2 March 2009

Accepted 3 March 2009

Available online 21 March 2009

Keywords:

Overflows

AMOC

Climate modeling

ABSTRACT

The overflows of cold, heavy waters from the Nordic Seas across the Greenland–Iceland–Scotland Ridges are simulated using the Hybrid Coordinate Model in a North Atlantic configuration. Results at three different horizontal model resolutions are compared to each other, to recent hydrographic sections and moored observations. Simulations in the finest grid employed, $1/12^\circ$ resolution, show realistic overflow pathways, reasonable overflow and Deep Western Boundary Current mean velocities and transports, and overall reasonable North Atlantic three-dimensional temperature and salinity fields, namely the Atlantic Meridional Overturning Circulation (AMOC). In contrast, simulations at coarser grids of $1/3^\circ$ and 1° resolution exhibit a range of significant problems owing to unresolved, dynamically vital features in the sea-floor topography. This lack of resolution, for example of the Faroe Bank Channel, leads to unrealistic overflow pathways between Iceland and Scotland in the $1/3^\circ$ and 1° cases. Accordingly, overflow mass transports are also unrealistic in this area. In the Denmark Strait Overflow the underlying topographical scales are larger, and pathways are reasonable even at coarse resolution. However, overflow speeds are too small in the $1/3^\circ$ and 1° cases. Underestimated velocities in the 1° simulations are compensated by an overestimated sill cross-section, whereas it is too small in $1/3^\circ$. As such, the $1/3^\circ$ and 1° simulations show both large under- and overestimations of volume transport at several locations. No significant improvement in modeled overflows takes place when the grid spacing is decreased from 1° to $1/3^\circ$. An experiment conducted with hand-tuned topography shows improved volume transports near the regions of modification, but somewhat increased errors in other parts of the deep circulation, indicating the complex response of the system to perturbations in bathymetry. These results demonstrate the importance of an accurate representation of the domain geometry, in particular the channels of the complex Iceland–Scotland ridge system, in order to reproduce the pathways of the deep AMOC.

© 2009 Elsevier Ltd. All rights reserved.

1. Introduction

On a background of climate and climate change, the Atlantic Meridional Overturning Circulation (AMOC) represents a key physical process. The AMOC is thought to affect such important conditions as the comparatively warm climate of Northern Europe and to be sensitive to global warming, possibly even to the point of shut-down as an extreme case (Hansen et al., 2004; Quadfasel, 2005; Bryden et al., 2005; Broecker, 2003; Häkkinen and Rhines, 2004; Wunsch and Heimbach, 2006; Cunningham et al., 2007; Kanzow et al., 2007). Hence, there is great interest in the AMOC and in modeling it (Bentsen et al., 2004; Gregory et al., 2005; Lumpkin and Speer, 2007). The warm branch of the AMOC transports

water between Iceland and Scotland northward at relatively shallow depths into the Nordic Seas, where it is cooled and transported to depth (Weaver et al., 1999; Blindheim and Francisco, 2004). The cold return branch has to cross over the Greenland–Iceland–Scotland ridge system (GIS). The flow then converts to overflows – gravity currents – on its southern side. These latter “Nordic Overflows” are the topic of this paper. It needs to be mentioned that deep water formation in the Labrador Sea is also part of the downward branch of the AMOC. Much of the cold water from the overflows and the Labrador Sea flows south on the western side of the North Atlantic as deep boundary currents (Fischer et al., 2004).

This study is conducted within the framework of the Climate Process Team on Gravity Current Entrainment (Legg et al., in press), a project aimed at improving the numerical simulation of gravity currents in global climate models. Within this context, we are asking the question of what the effect of the horizontal model resolution is on numerically simulated Nordic Overflows and other aspects of the North Atlantic circulation. This question is motivated

* Corresponding author. Tel.: +1 305 421 4189.

E-mail addresses: ychang@rsmas.miami.edu (Y.S. Chang), zgarrafo@rsmas.miami.edu (Z.D. Garraffo), hpeters@esr.org (H. Peters), tozgokmen@rsmas.miami.edu (T.M. Özgökmen).

by a current typical horizontal grid spacing in global climate models of 1° – which is comparable to, and sometimes far greater than the width of most overflows.

This is of course not the first investigation of the effect of horizontal resolution on overflow models. For example, Chang et al. (2008) found that the pattern and pathways of the Red Sea Overflow do not become realistic until the detail of the bottom topography is resolved. In that case the key topographic features are two channels that are 2–5 km wide. Among several studies to examine topographic influences on overflows and AMOC structure, Roberts and Wood (1997) performed sensitivity tests with a 1° model by artificially changing sill depths in the Denmark Strait as well as in the Iceland–Scotland ridges. The simulations across the entire domain from the Nordic Seas to the subpolar gyres proved to be highly sensitive to topographic variations. Similar results were obtained by Beismann and Barnier (2004) in an investigation of the strength of the AMOC as a function of topographic differences near the sills of the Nordic Overflows.

Herein, we are studying overflows, the AMOC and, more generally, wide aspects of the circulation in the subpolar and Nordic Seas as a function of horizontal model resolution. We are focusing on numerical simulations with a community ocean general circulation model, routine atmospheric forcing, routine initialization, and routine procedures for generating the model seafloor topography at various resolutions. There are other approaches to overflow modeling, such as the Marginal Sea Boundary Condition (MSBC). In this approach, the exchange between the marginal sea and the open ocean, descent and entrainment of the outflow on the continental slope are collapsed into what amounts to a side-wall boundary condition for an ocean general circulation model. This approach to modeling deep water formation by a marginal sea is appropriate from an oceanic perspective since the outflow water mass transformation takes place within one grid cell of a typical ocean climate model. The reader is referred to Price and Yang (1998) for details. In MSBC, the overflows are not explicitly simulated, and this type of parameterization is shown to be effective in coarse-resolution studies, in particular when the outflow from the marginal sea remains as a single branch before equilibrating in the open ocean, such as in the case of the Mediterranean outflow (Wu et al., 2007; Xu et al., 2007).

In light of the importance of overflows from Nordic Seas on the AMOC, and their complex structure, we pose the following questions:

- Can we obtain realistic Nordic Overflows and deep transport pathways using ocean general circulation models, in which the overflows are explicitly simulated?
- If so, at which model horizontal resolution is this achieved?

Experiments are conducted by gradually increasing horizontal resolutions. We start with 1° grid, which appears to be the typical ocean model resolution used in climate studies at the present time (e.g. Gnanadesikan et al., 2006). Then, we carry out simulations at $1/12^\circ$ grid spacing, which resolves the most important topographic features, as well as many mesoscale turbulent eddies, jets and western boundary currents. A simulation at an intermediate, eddy-permitting resolution of $1/3^\circ$ complements the other two. We are striving to trace the pathways of all components of the Nordic overflows and of the AMOC in the North Atlantic in good detail.

The paper is organized as follows. The principal properties of the Nordic Overflows are reviewed in Section 2. The model configuration, initialization, atmospheric forcing, bottom topography and model parameters are laid out in Section 3. The results of the simulations, including detailed comparisons with moored observations and hydrographic sections follow in Section 4. The paper concludes with summary and discussion.

2. Review of Observations on Nordic Overflows

The Greenland–Iceland–Scotland ridge system is a continuous, relatively shallow barrier which constrains the exchange of waters between the subpolar North Atlantic and Nordic Seas (Fig. 1). Sill depths at various locations range from 300 to 840 m. Iceland and the Faroe Islands divide the ridge into three gaps that are the main routes for the exchange between the water masses in the North Atlantic and Nordic Seas (Hansen and Østerhus, 2000). The fairly wide Denmark Strait (DS) is the westernmost gap with a sill depth of about 600 m. The rather dense Denmark Strait Overflow Water (DSOW) crosses the sill and continues southwestward and downward as illustrated in Fig. 1. Maximum speeds at the sill can exceed 0.5 m s^{-1} (Macrander et al., 2007). The corresponding DSOW mass transport is 2.7–2.9 Sv at the sill (Dickson and Brown, 1994; Hansen and Østerhus, 2000; Girtton et al., 2001; Macrander et al., 2007). From the sill, the DSOW continues to flow through the Irminger Basin parallel to the east coast of Greenland southwestward and downward on a broad slope. Entrainment of ambient fluid along this path increases the overflow transport to ~ 13.3 Sv at the southern tip of Greenland (Dickson and Brown, 1994). The DSOW then joins the deep water circulation in the Labrador Sea, where deep-convection processes increase the transport of this main return branch, the Deep Western Boundary Current (DWBC), to about 17 Sv near the Grand Banks (Fischer et al., 2004).

The middle gap in the GIS ridges is the Iceland–Faroe Ridge (IFR), which is broad and shallow with crest depths of 300–500 m. Since it was first probed more than a century ago by Knudsen (1898) a multitude of observations of the overflow across the IFR have been made (Tait, 1967; Steele, 1967; Meincke, 1974). However, because the IFR is broad and long and has highly-variable flow, the detail and overall magnitude of the overflows are still uncertain. The transport is estimated to be no more than 1 Sv. After crossing over the IFR, overflow waters flow mainly southwestward along the Iceland Basin (Fig. 1).

The easternmost gap on the GIS is the Faroe–Shetland Channel, which has a relatively deep sill about 1000 m deep. This channel is blocked at its southwestern end by the Wyville–Thomson Ridge (WTR) with a sill depth not deeper than 600 m. The Wyville–Thomson Ridge joins the Scottish shelf at its southern end and Faroe Bank at its northern end. The Faroe Bank is separated from the Faroe Plateau by the narrow and deep Faroe Bank Channel (FBC), which has a sill depth of 840 m. Because of its depth the FBC is the main outlet from the Faroe–Shetland Channel (FSC) and a major outlet from the Nordic Seas. Numerous observations in the FBC indicate maximum velocities up to $\sim 1 \text{ m s}^{-1}$ (Mauritzen et al., 2005; Geyer et al., 2006). The reported volume transport from this channel is 1.5–2.1 Sv (Hansen and Østerhus, 2000; Lake and Lundberg, 2006; Geyer et al., 2006). After the overflow water passes through the FBC, a considerable part crosses the Island Basin and joins with the overflows that have crossed over the Iceland–Faroe Ridge (Steele, 1961; Swift, 1984; Saunders, 1996; van Aken, 1998; Hansen and Østerhus, 2000). Further on, the overflow water continues southwestward along the Iceland Basin and eventually reaches the Mid Atlantic Ridge. It flows southward along its eastern flank until parts of it escape into the Irminger Basin through the Charlie–Gibbs Fracture Zone (CGFZ; Saunders, 1994) and probably other gaps in the Mid Atlantic Ridge. The overflow water that crosses over the Wyville–Thomson Ridge continues flowing southward through the Rockall Channel along the eastern flank of the Rockall–Hatton Plateau (Ellett and Roberts, 1973; Sherwin and Turrell, 2005). Estimates of the overflow transport in this region are rather uncertain with a wide range of reported values between 0.1 and 2 Sv.

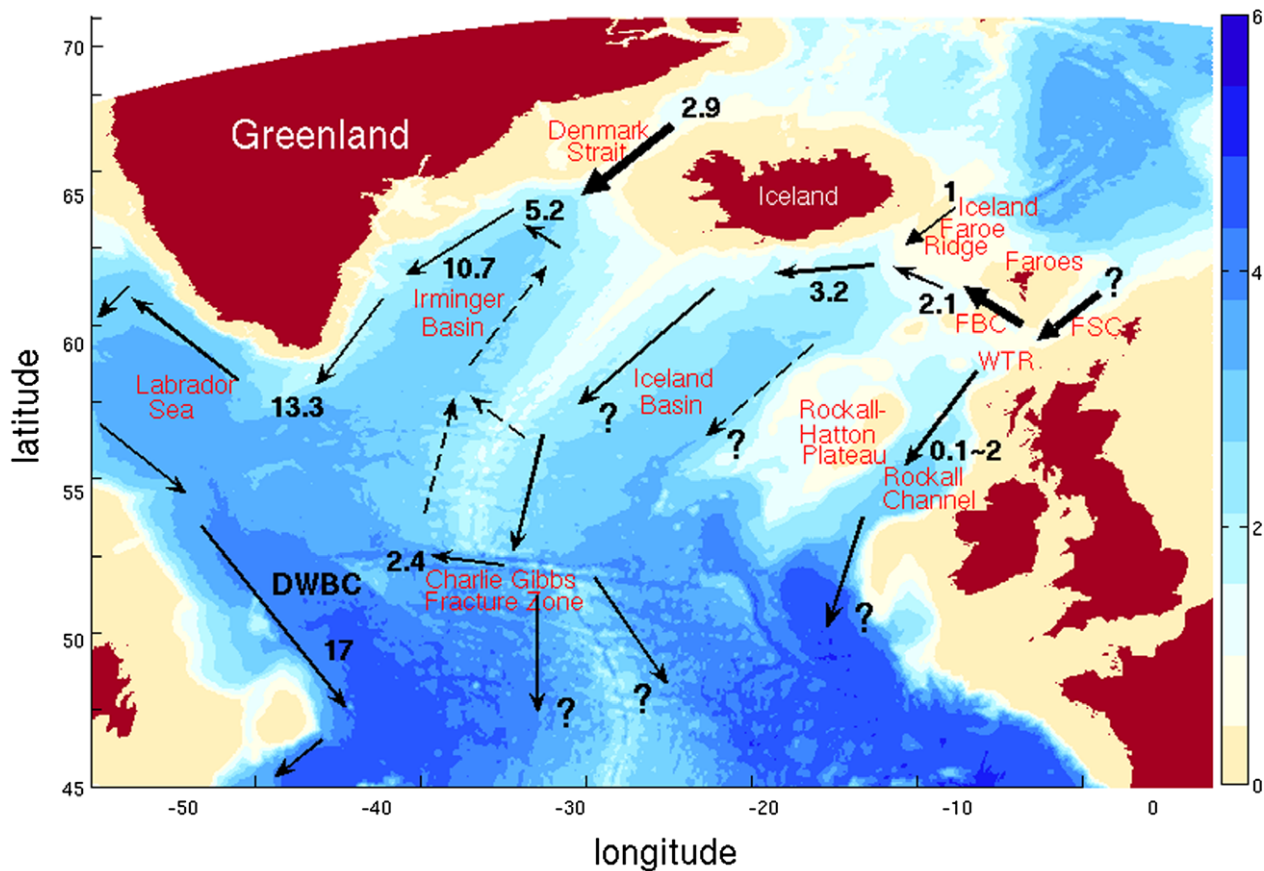


Fig. 1. Schematic of North Atlantic overflows. Solid arrows, observed overflows and their directions; thick arrows, main primary overflows; dashed arrows, presumed overflows and directions; numbers, mass transports in Sv from observations; question marks, unknown mass transports. The colorbar indicates water depth in km. (For interpretation of the references to colour in this figure legend, the reader is referred to the web version of this article.)

The long distance spreading of overflow waters which have crossed over the GIS is better known in the western North Atlantic than in the basins east of the Mid Atlantic Ridge as indicated by dashed lines and question marks in Fig. 1. Pathways and transports of overflow waters south of Rockall Channel as well as possible flows on the western side of Rockall Plateau remain unknown. Further, the southwestward transport magnitude along the eastern flank of the Mid Atlantic Ridge is unclear, as are the transports through gaps in the Ridge with the exception of the flow through the CGFZ of about 2.4 Sv (Saunders, 1994). Comparing this value with a westward overflow water transport of 3.2 Sv south of Iceland (Saunders, 1996) suggests that some overflow water crosses westward into the Irminger Basin north of the CGFZ. Possibly there are other branches of spreading overflow water that flow southward on either or both sides of the Mid Atlantic Ridge south of the CGFZ.

3. The numerical model and configuration

We use the Hybrid Coordinate Ocean Model (HYCOM, Bleck, 2002; Chassignet et al., 2003; Halliwell, 2004). Most relevant for this study is the Lagrangian nature of isopycnic coordinates to naturally migrate with the interface between the descending gravity currents and the ambient fluid, thereby allocating vertical resolution to locations where most of the entrainment tends to take place. This desirable behavior of isopycnic coordinates in HYCOM was shown to be advantageous in previous simulations of gravity currents (Chang et al., 2005; Xu et al., 2006; Xu et al., 2007; Chang et al., 2008).

Previous studies of the North Atlantic with HYCOM have employed a model domain ranging from latitudes 20°S to 70°N. Herein, we have extended the domain northward, namely to 80°N in 1/12° and 1°, and to 77°N in 1/3° cases, so that more of the Norwegian Sea is covered by the model. We employ three different horizontal grid resolutions of 1/12°, 1/3°, and 1° grids. The coarsest 1° grid corresponds to the typical resolution of current global coupled climate models. The finest 1/12° grid resolves not only the most essential details of the seafloor topography, but also most of the meso-scale eddies in the circulation. Finally, the 1/3° grid is selected as the middle course between the other two.

The model seafloor topography is a crucial aspect of this study. The following paragraph describes effects of varying grid resolutions as well as the methods of deriving topographies at varying resolution. Fig. 2a provides an overview over the important part of the model domain while the subsequent panels (b–d) depict the complex terrain between Iceland, the Faroe Islands and Scotland at the three resolutions of 1/12°, 1/3°, and 1° chosen herein. The 1/12° grid clearly captures the key features, especially the narrow Faroe Bank Channel (Fig. 2b). In 1/3°, channels such as the FBC are still roughly expressed, however, the FBC is represented by only two grid points, and its sill depth has become ~200 m shallower than at 1/12°. In the 1° most channels and banks are no longer discernible. The FBC, for example, has simply vanished. Moreover, the 1° topography has an unrealistically deep channel across the Iceland-Faroe Ridge just southeast of Iceland at ~63.5°N. This artifact is a result of the standard procedure of generating bottom topographies in HYCOM. First, the bathymetric data from DBDB2 is projected to the grid space using spline interpolation. Then, a

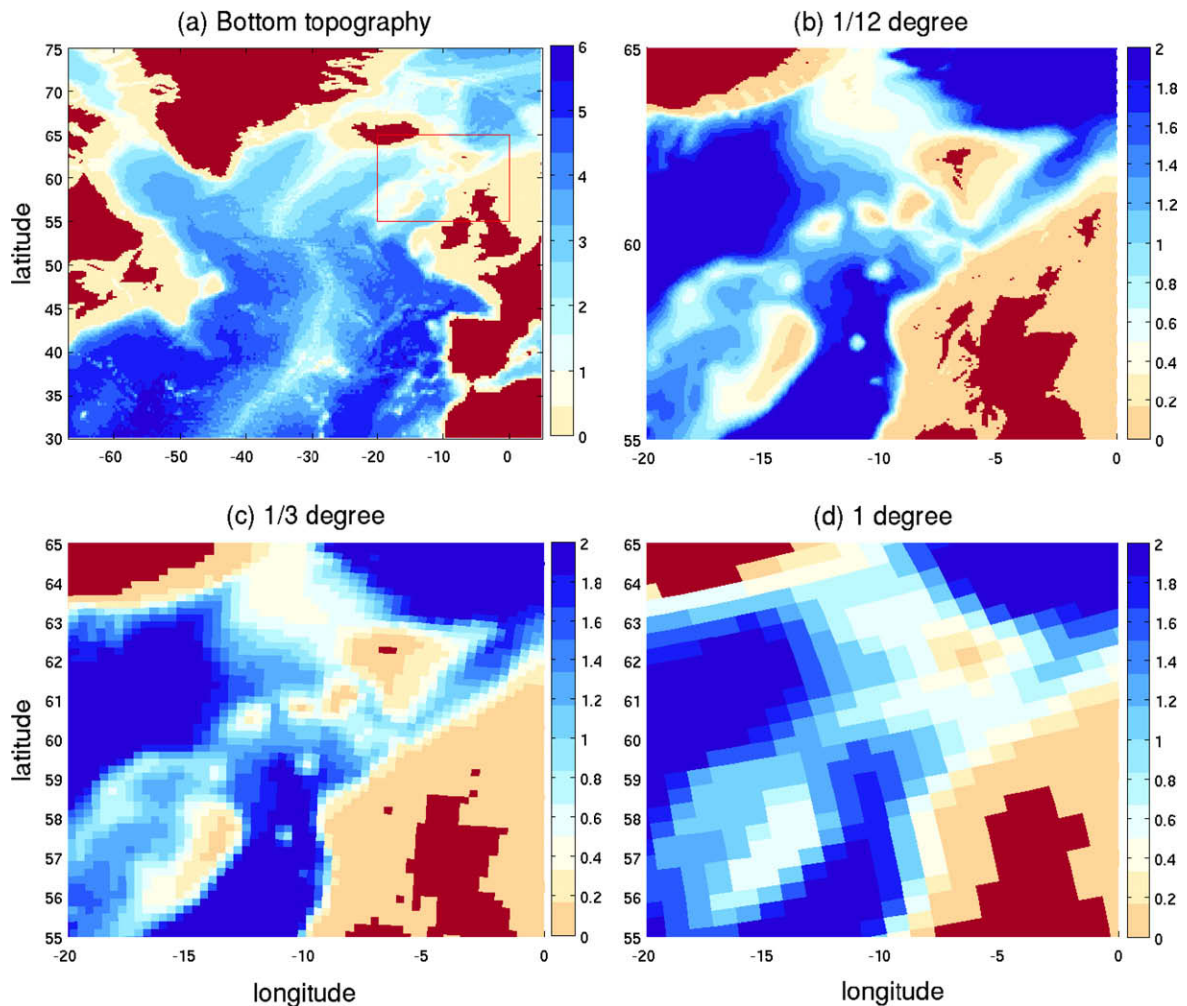


Fig. 2. Seafloor topography: (a) part of the model domain from the subtropical North Atlantic to the Norwegian Sea; (b) magnified domain between Iceland and Scotland at 1/12° resolution. The narrow channels of both Faroe-Shetland Channel and the Faroe Bank Channel are resolved. (c) The same area at 1/3° resolution. The Faroe-Shetland Channel is resolved but not the FBC. (d) Ditto, 1° resolution. Neither the Faroe-Shetland Channel nor the FBC are resolved. The depth color scale is in km. (For interpretation of the references to colour in this figure legend, the reader is referred to the web version of this article.)

convolution with a spatial filter function (close to a Gaussian filter) is applied once.

The simulations of each grid were initialized by slightly different climatological data sources, namely GDEM3 (Teague et al., 1990) for the 1° and 1/12° simulations and Levitus (Levitus et al., 1994; Levitus and Boyer, 1994) for the 1/3° case. This has no significant difference in outputs at least in terms of the initial conditions. In all simulations, the mechanical and thermodynamic atmospheric forcing at the sea surface is given by monthly mean data from the ECMWF 40-Year Reanalysis (ERA-40) Data Archive (Uppala et al., 2005), but in the 1/12° case 6-h climatological anomalies were added to the mechanical forcing. Vertical turbulent mixing is parameterized by the KPP algorithm (Large et al., 1994). Along the northern and southern boundaries, temperature, salinity and pressure are relaxed to climatology within sponge zones, the details of which are as follows. In the 1° case, the northern (southern) buffer zone is taken as 19 (10) grid points, in which the relaxation (*e*-folding) time scale function changes linearly from 48 to 6 days toward the boundaries. In the 1/3° case, the northern (southern) buffer zone is taken as 15 (50) grid points, and the relaxation time scales are the same, 48 to 6 days. In the 1/12° case, the northern buffer zone contains 103 points with a relaxation time scale of 30 to 5 days, while the southern buffer zone has 43 points with times scales of 60 to 10 days. The influence of the

northern buffer zone on the internal circulation in the Nordic Sea is reduced by extending the domain boundary northward with respect to those chosen in previous simulations with HYCOM or its earlier version MICOM (Miami Isopycnal Coordinate Ocean Model; for instance 65°N in (Garraffo et al., 2001, and 70°N in Chassignet et al., 2007). The southern boundary is not very critical as we focus our attention on the deep sub-polar circulation here on time scales smaller than the North Atlantic overturning circulation. The simulations were integrated for 6 years to allow the model to attain a stable state with quasi steady state in the overflows. Both the atmospheric forcing and the initial stratification are broadly representative of the North Atlantic state of the late twentieth century. The same holds for our simulations, an important factor in comparisons with ocean observations.

4. Results

4.1. Overflow pathways and effects of the model topography

The main objective of this study is to address the question of whether we can successfully simulate the complicated pattern of Nordic Overflows as they are observed in Fig. 1, and if so, at what grid resolution. Among the numerous branches of the Nordic Overflows we focus on its two main branches, the overflows through

the Denmark Strait and through FBC. These carry the majority of overflow water into the subpolar North Atlantic. While the Denmark Strait has simple topography and overflow pathway, the complex topography and curved and bifurcated overflow pathways of the Faroese Channels pose much more of a challenge. Here, we expect high sensitivity to the bottom topography, and therefore we focus our attention on this area in the following.

The propagation pattern of overflows between different grids in the eastern North Atlantic are compared in Fig. 3. It shows the initial temperature (T) distributions on HYCOM model layers representative of overflow waters and the evolution at five time steps of 0, 1, 7, 13 and 19 months in the form of deviations from the initial T -fields. The overflow layers are distinguished from the others using the criterion of $\sigma_\theta \geq 27.8$. Fig. 3 shows clear and strong differences in the propagation pattern on the three model grids which increase with time, being small at one month evolution time and quite dramatic already at 7 months.

In the 1° grid most of the cold water from the Nordic Seas enters the subpolar North Atlantic over the wide and shallow Iceland–Faroe Ridge instead of passing through the narrow and deep Faroe Bank Channel. This result is evident a-priori to the computation

based on the lack of resolution of the FBC at 1° depicted in Fig. 2 and discussed in Section 2. As the overflow cannot find its path through Faroe–Shetland Channel and FBC, the cold water masses are pushed south over the much wider IFR, especially through the artificial depression in the Iceland–Faroe Ridge just southeast of Iceland created by the seafloor algorithm as discussed above. Thus, the overflow over the Iceland–Faroe Ridge is overestimated at 1° , while the overflow through the FBC is underestimated owing to the poor grid resolution. These overflow waters in the 1° simulation flow southward along the eastern side of the Mid Atlantic Ridge and eventually split into one branch flowing westward through the Charlie Gibbs Fracture Zone and another branch that continues southeastward along the Mid Atlantic Ridge.

The overflow propagation pattern is quite different in the $1/3^\circ$ grid (Fig. 3). Here, the majority of the overflows mass passes through the Faroe–Shetland Channel rather than over the Iceland–Faroe Ridge as in the 1° case. However, after passing through the Faroe–Shetland Channel most of the overflow water keeps a southward direction over the Wyville–Thompson Ridge, and only a small part turns toward the northwest in trying to pass through the partially blocked FBC. The water that crosses over the shallow

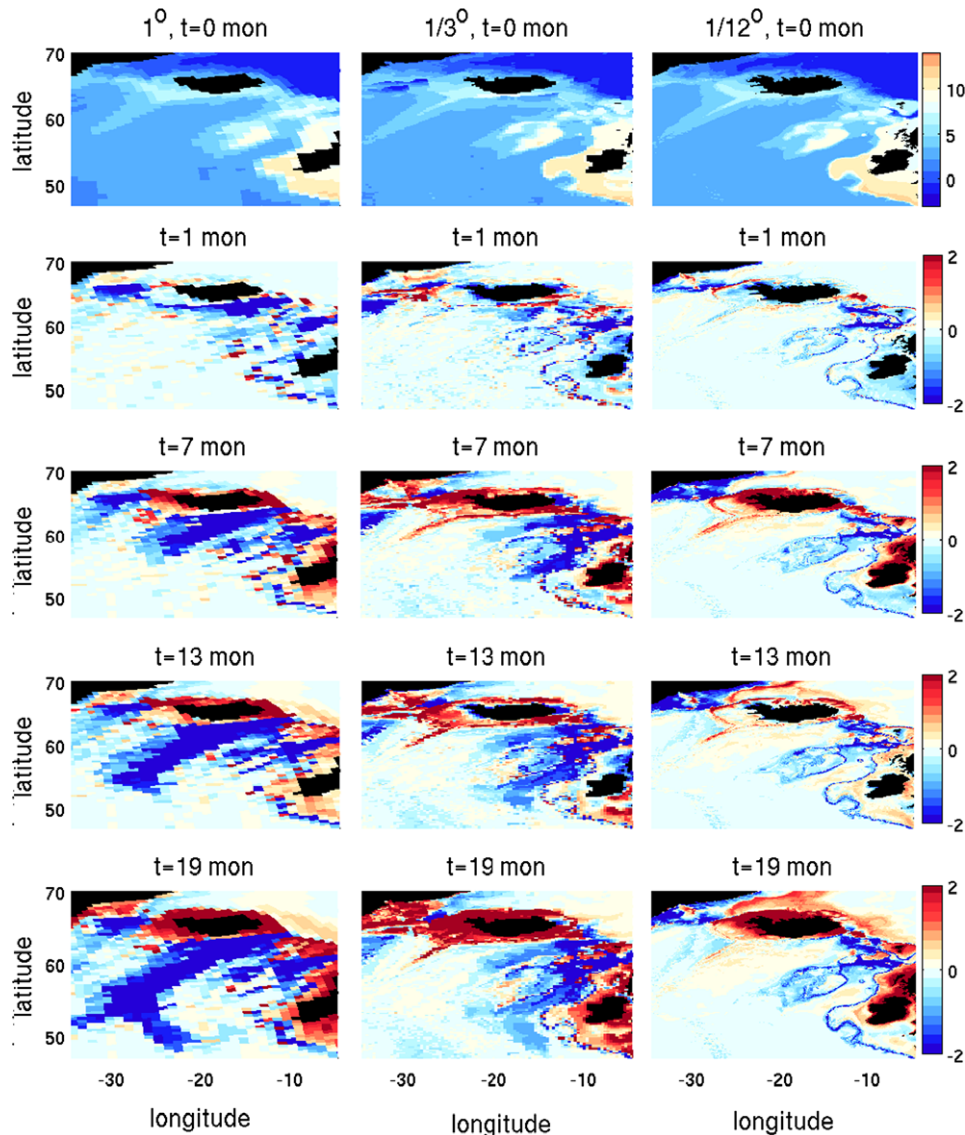


Fig. 3. Plan views of the time evolution of the overflow propagation between Iceland and Scotland in a comparison of the 1° , $1/3^\circ$ and $1/12^\circ$ simulations. Plotted are temperature contours (in $^\circ\text{C}$) at the start of the simulations and temperature anomalies, deviations from $t = 0$, thereafter at $t = 1, 7, 13, 19$ months.

Wyville-Thompson Ridge continues to the southwest and occupies most part of the Rockall Channel. Even though part of the overflow pathways in $1/3^\circ$ grid are more realistic than in the 1° grid, they still disagree with the observations. Most of the overflow water still end up in the wrong ocean basin as shown by a comparison of Figs. 3 and 1 and noting a transport of 2 Sv through the FBC and about an order of magnitude less across the Wyville-Thompson Ridge. Hence, even a resolution of $1/3^\circ$ is insufficient to capture the most basic properties of the Nordic Overflows.

In the finest grid of $1/12^\circ$ there are no unrealistically strong currents over either the Iceland-Faroe Ridge or the Wyville-Thompson Ridge. Instead, the overflow is concentrated in the Faroe Bank Channel, as it should be. In the $1/12^\circ$ panels of Fig. 3 the overflow waters seem to proceed westward after passing through the Faroese channels, although this flow is not so clearly seen compared to the other two coarser grids. More details about this flow pattern are discussed in Fig. 4.

In order to investigate the overflow pathways at different grid resolutions in more detail, we now discuss four regions of special interest in conjunction with Figs. 4–7. These depict the overflow layer temperature fields in the regions of the Faroe Islands, Iceland Basin, Irminger Basin, and the Labrador Sea, respectively. Model output averaged over the sixth year of integration are shown as bottom temperature fields with superimposed current vectors.

In Fig. 4 the overflows in the Faroe Islands areas are compared among the different grids in panels (b) through (d) while the bottom topography at $1/12^\circ$ grid is shown in panel (a). As already found in Fig. 2, each grid has a different overflow pathway. The major flow pathways found above are confirmed in Fig. 4 by the cur-

rent vectors. To reiterate, in 1° the major flow is across the Iceland-Faroe Ridge just southeast of Iceland continuing southwestward along the southern coast of Iceland and the Mid Atlantic Ridge. In $1/3^\circ$ the major flow is through the Faroe-Shetland Channel, across the Wyville-Thompson Ridge and into Rockall Basin. In $1/12^\circ$, finally, the major flow takes the route of the Faroe-Shetland Channel and Faroe Bank Channel continuing westward toward Iceland and the Mid Atlantic Ridge. Obviously, in this region of complex topography with small scales the model seafloor topography is the major factor that controls the simulated overflows.

We are unable to validate part of the overflow pathways for lack of observations in large parts of the North Atlantic. This holds for the area east and west of the Mid Atlantic Ridge south of Iceland and south to the Charlie Gibbs Fracture Zone (CGFZ) and beyond (Fig. 5). Fig. 1 indicates quantitative information only at the exit from the FBC and from the Iceland-Faroe Ridge in the northeast and in the CGFZ in the south (Saunders, 1994, 1996). Hence, we can only partly evaluate and compare model performances as depicted in Fig. 5. A prominent feature in the 1° simulations is the strong flow of cold overflow water along the southeastern and eastern flank of the Mid Atlantic Ridge to the CGFZ and beyond (Fig. 5b). This flow is the continuation of the excessive flow over the Iceland-Faroe Ridge discussed above and illustrated in Fig. 4b. Only part of the flow along the Mid Atlantic Ridge turns west in the CGFZ. This contrasts with the $1/3^\circ$ and $1/12^\circ$ simulations in which the southwestward flow of overflow water is generally weaker and warmer, and in which most of it does not reach the CGFZ (Fig. 5c and d). Apparently, the overflow pathway crosses westward over the Mid Atlantic Ridge well north of the CGFZ. We note that all resolutions show

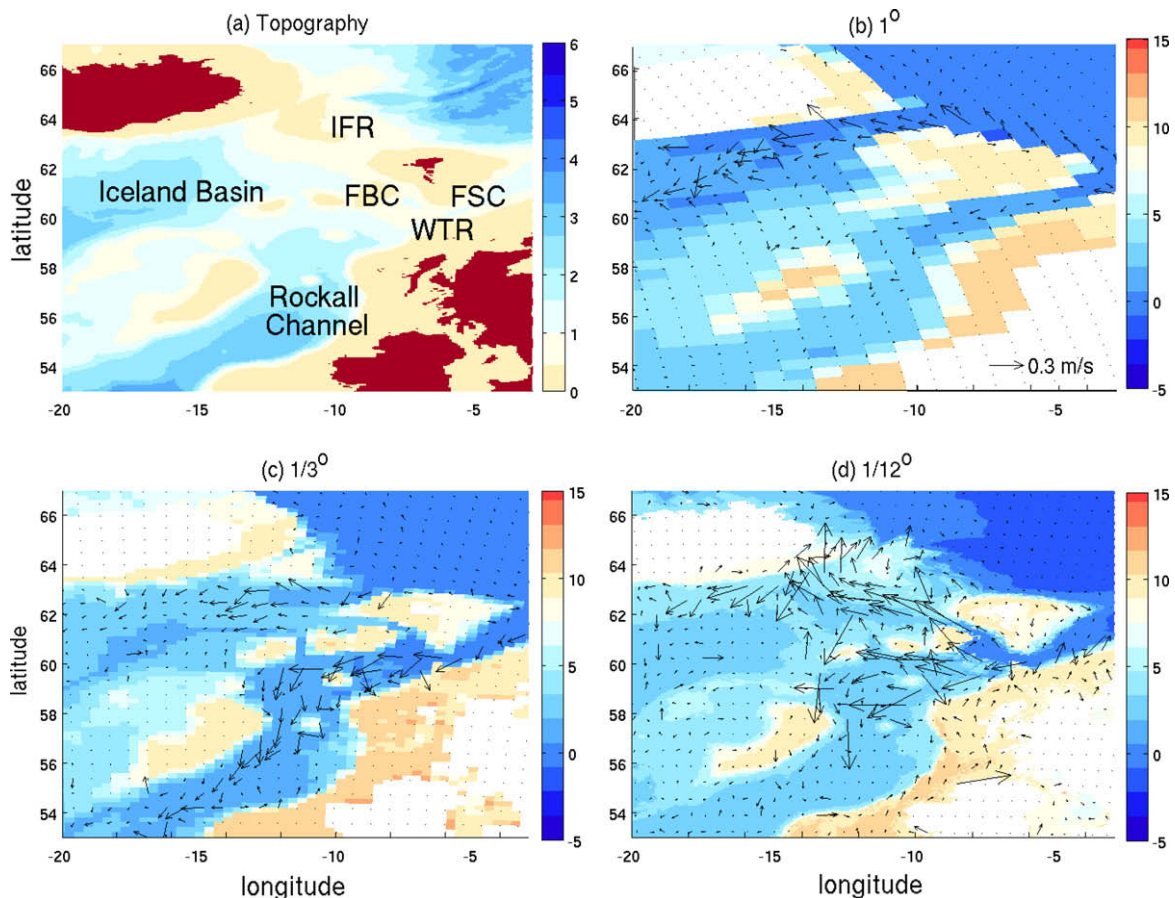


Fig. 4. Seabed topography and the overflow pattern between Iceland and Scotland. (a) Model bottom topography at $1/12^\circ$. (b) Temperature distribution with velocity vectors in the “overflow” layer from the 1° simulation; (c) $1/3^\circ$ simulation; (d) from $1/12^\circ$.

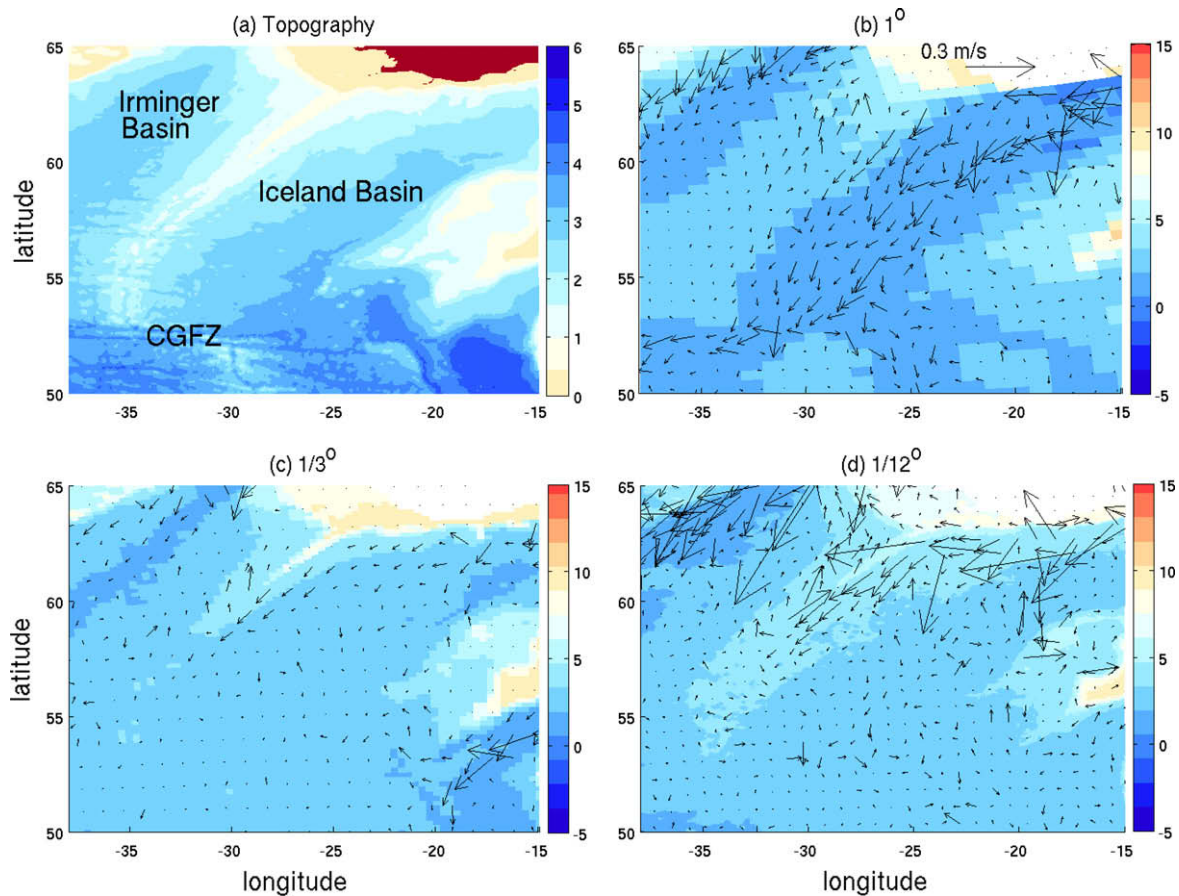


Fig. 5. Seabed topography and overflow pathways around the Mid Atlantic Ridge south of Iceland; as Fig. 4: (a) bottom topography, (b) temperature distribution with velocity vectors from 1° , (c) from $1/3^\circ$, (d) from $1/12^\circ$.

northeastward flow along the northwestern flank of the Mid Atlantic Ridge which eventually flows toward the sill of Denmark Strait. To our knowledge, there are no observations to confirm this result. Similarly, we cannot completely discount the southward flow south of the CGFZ in the eastern North Atlantic Basin in the 1° simulations (Fig. 5b).

About 60% of the dense water masses crossing the Greenland–Iceland–Scotland ridges are carried by the Denmark Strait Overflow. As already shown in Fig. 1, the straightforward path of the latter from the sill of Denmark Strait is along the eastern shelf off Greenland. Fig. 6 shows the model results of overflow pathways and velocities in this region. Unlike previously discussed areas further east, the overflow pathways are similar between all the three grids. However, in the 1° and $1/3^\circ$ simulations the coldest water lies east of the velocity maximum, which is situated above the continental slope. In contrast, the western edge of the cold water and maximum flow coincide in the $1/12^\circ$ case.

After the overflows reach the southern tip of Greenland, they turn to the northwest and enter the cyclonic deep water circulation in the Labrador Sea. The patterns of the deep, cold flow between southern Greenland and the Grand Banks generally agree among the three different grids as seen in Fig. 7. However, the 1° simulations show comparatively weak currents except on the north side of the Grand Banks. In contrast, currents in the $1/12^\circ$ are comparatively swift and narrow. At the exit of the Labrador Sea at the Grand Banks, the main pathways of flows in all three grids become complicated to trace further. This could be associated with the sharp bend in topography, which induces at least in the $1/12^\circ$ case the break down of the flow field into eddies. Schematics of the gen-

eral circulation appear to indicate a bifurcation of the deep flow field near the Grand Banks (e.g., Schmitz, 1996, Fig. I-86). A recent analysis of acoustically-tracked RAFOS float trajectories shows that the vast majority of floats released near 50°N leave the DWBC by the tail of the Grand Banks at 43°N , where some take a path towards the CGFZ whereas others drift along the western flank of the Mid Atlantic Ridge towards the subtropics (Bower et al., submitted for publication). This is certainly an interesting problem, but in this study, we restrict the analysis of the model fields to sub-polar Atlantic in order to preserve our focus on Nordic Overflows.

4.2. Comparison with observations

We now proceed to a comparison of our simulations with the observations. We compare the water mass structure from some hydrographic sections, velocity and temperature profiles and the transport magnitude of overflow waters from a number of moored current meter arrays. As mentioned at the end of Section 3, our simulations are roughly representative of mean conditions in the late 20th century. In contrast, the observations were taken at specific times and are thus subject to ocean variability on a variety of time scales. The moorings were deployed for 1–6 years. Averaging over these time spans reduces the seasonal variability and some interannual variations.

The observational data sets chosen herein are listed in Table 1, and their locations are marked in Fig. 8 as P1–P10. The available data at each location are denoted by 'T' for the temperature profiles, 'V' for the velocity profiles, 'Sec.' for the cross-sectional maps, and 'Tr' for the mass transport.

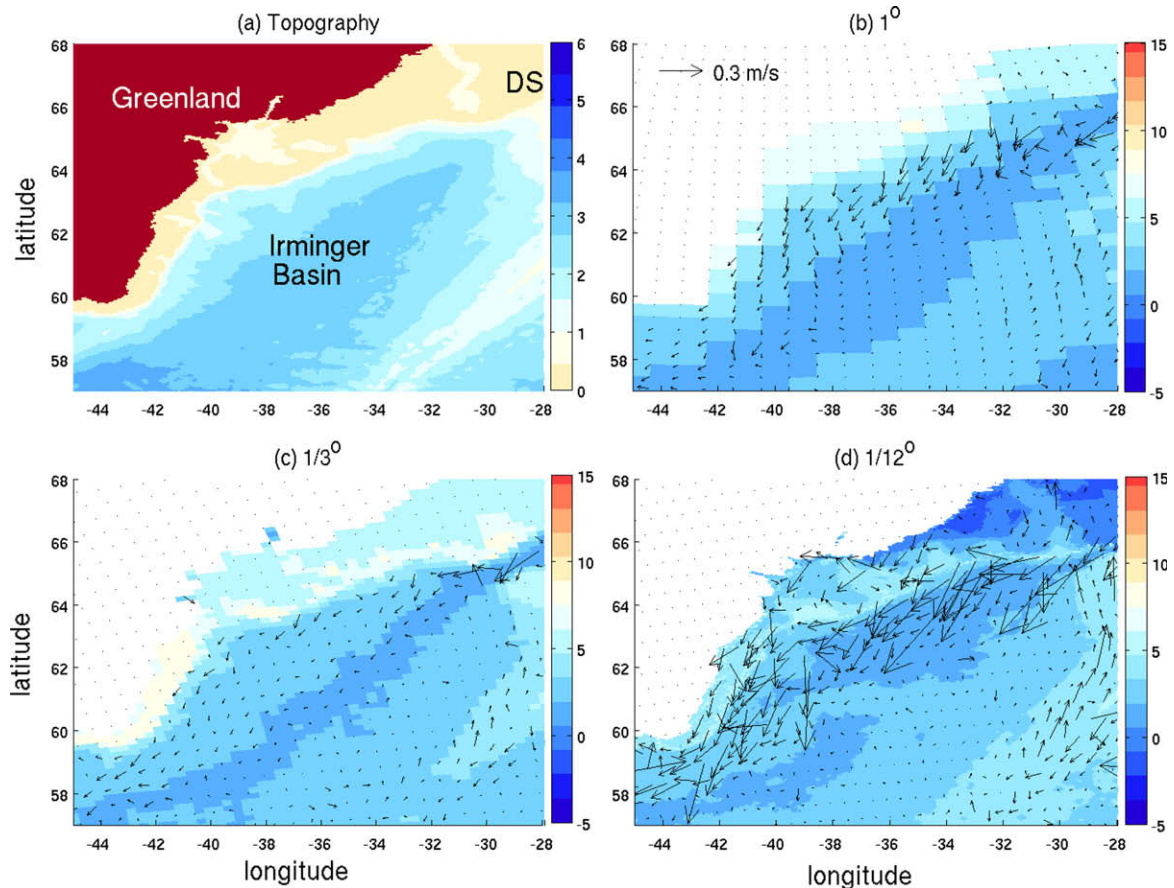


Fig. 6. Seabed topography and overflow pathways in the Irminger Basin; as Fig. 4: (a) bottom topography at $1/12^\circ$, (b) temperature distribution with velocity vectors from 1° , (c) from $1/3^\circ$, (d) from $1/12^\circ$.

4.2.1. Comparison with hydrographic sections

In Figs. 9–11, we compare density or temperature sections across overflows between simulations and observations at the sill of Denmark Strait (P1 in Fig. 8), in the Faroe-Shetland Channel (P5), and the FBC (P6). Potential density (σ_θ) contours across Denmark Strait show the overflow water banked over the northwestern slopes with a sharp front just east of the deepest point (Fig. 9a; Macrander et al., 2007). This spatial pattern is nicely replicated in the $1/12^\circ$ simulations except that the simulated area of DSOW is larger than in the observations (see the heavy black line in Fig. 9a and b). The agreement between observations and simulations is worse for the coarser grids. In the $1/3^\circ$ grid the distribution pattern is qualitatively correct with overflow water on the northwest side, but the amount of DSOW is smaller than in the observations and the $1/12^\circ$ simulations (Fig. 9c). This is at least partly an effect of a sill depth of only 600 m in the $1/3^\circ$ grid compared to 680 m in the $1/12^\circ$ grid. In the 1° grid the channel is resolved by only 2–3 grid points (Fig. 9d). The deepest part is far too wide at 100 km, one grid cell, and the shape of the channel is not well represented. Consequently, the area occupied by DSOW is too large compared to the observations.

The simulations on the coarser grids show similar problems in the cases of the Faroe-Shetland Channel (P5 in Fig. 8) and the Faroe Bank Channel (P6). The observed potential temperature section across the Faroe Shetland Channel (Mauritzen et al., 2005) shows a modestly inclined interface on top of the overflow water (Fig. 10a). This feature is well-simulated in the $1/12^\circ$ and $1/3^\circ$ grids (Fig. 10b and c). However, while the $1/12^\circ$ replicates the shape of the channel well, it is too deep in its eastern part in $1/3^\circ$. In con-

trast, there is almost no channel in the 1° grid, depths being far too shallow throughout the section (Fig. 10d). There is only a very small area of overflow water in this case. The situation is even worse in the Faroe Bank Channel (Fig. 11). There hardly is any channel in $1/3^\circ$ and none in the 1° grid, which also shows no dense water at all. In contrast, the $1/12^\circ$ simulation replicates the channel shape and the spatial overflow water distribution well.

4.2.2. Comparison of velocity and temperature profiles

A further assessment of the model performance is given by a comparison of observed and simulated velocity and temperature profiles shown in Figs. 12–17. North (V) and east (U) velocity components from Denmark Strait are depicted in Fig. 12. The simulated velocities from the $1/3^\circ$ and 1° grids are far too small at the overflow level near 500 m depth while the $1/12^\circ$ velocity profiles agree reasonably well with the observations. The depths of maximum flow speeds do not coincide between observations and simulations and between the different grids. This is a consequence of differences in the model seafloor topography and actual depths. Such differences are inevitable and not of further consequence. In the comparison with the observations one has to consider that the measurements were taken at one spot while the simulations represent averages over significantly large horizontal grid cells.

Figs. 13 and 14 depict velocity and temperature profiles, respectively, from locations P2, P3 and P4 in the Denmark Strait overflow area (see Fig. 8). Three moorings have been selected from the spatial arrays as indicated in the caption. The velocity vector has been rotated by -45° so that the new \tilde{V} component is in the streamwise

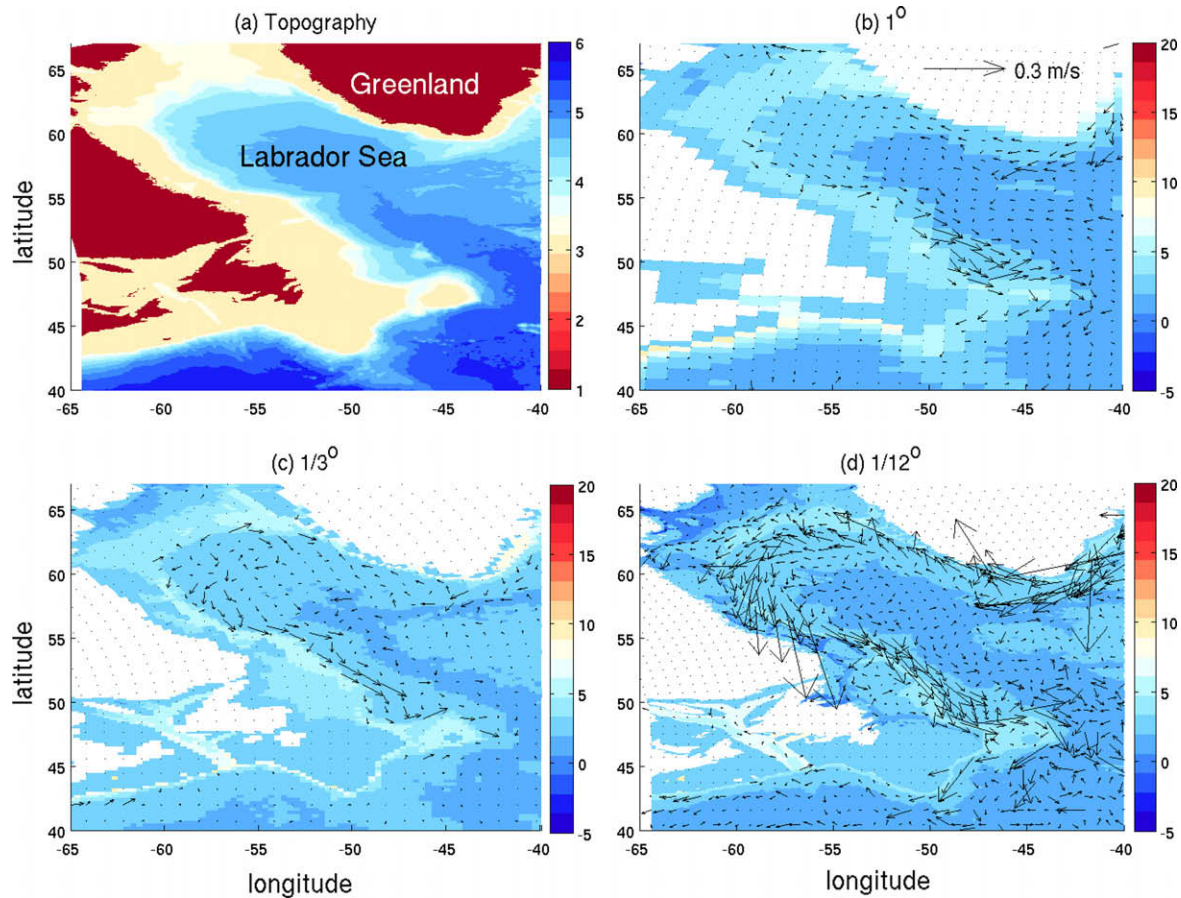


Fig. 7. Seabed topography and the overflow pattern near the Labrador Sea; as Fig. 4: (a) bottom topography, (b) temperature distribution with velocity vectors from 1° , (c) from $1/3^\circ$, (d) from $1/12^\circ$.

Table 1

List of the observational data used herein.

Locations	Source of the data	Time of deployment	Available data
P1: DS Sill	Mauritzen et al., 2005	1999–2000	'V','Sec','Tr'
P2: Exit of DS	Dickson and Brown, 1994	1986–1991	'T','V','Tr'
P3: Exit of DS	Dickson and Brown, 1994	1986–1991	'T','V','Tr'
P4: Exit of DS	Dickson and Brown, 1994	1986–1991	'T','V','Tr'
P5: FSC	Meincke, 1974	Jun., 2000	'Sec'
P6: FBC	Geyer et al., 2006	Sep., 2003	'Sec','Tr'
P7: Southeast of Iceland	Schmitz, 1996	1990–1992	'T','V','Tr'
P8: CGFZ	Saunders, 1996	1988–1989	'T','V','Tr'
P9: Exit of Labrador Sea	Fischer et al., 2004	1997–1999	'V','Tr'
P10: East of Grand Banks	Sherwin and Turrell, 2005	1993–1995	'V','Tr'

Notation: 'T': temperature profile; 'V': velocity profile; 'Sec.': hydrographic section; 'Tr': Mass transport; 'DS': Denmark Strait; 'FSC': Faroe-Shetland Channel; 'FBC': Faroe Bank Channel.

direction with negative values corresponding to the overflow. Similar to P1, the velocity magnitudes show reasonable agreement in the $1/12^\circ$ grid but are seriously underestimated by the $1/3^\circ$ and 1° grids. Some locations, such as P2 (Figs. 13 and 14a), have the additional problem that the coarse 1° bottom topography has depths much too shallow. Overflow velocities are smallest in the $1/3^\circ$ grid even though the topography fits fairly well with reality. Another significant feature of the modeled velocity profiles are their strong barotropic components. Observed profiles show near-bed maximum flow rates, but the modeled velocities at P3 and P4 have small vertical gradients throughout. The simulated temperature profiles are in better agreement with the observations than the velocities (Fig. 14). Except for P2, the temperature in the

bottom layer is in reasonable agreement with the observations within an error range of 1–2 °C. In the surface layers, however, there are large differences between the $1/12^\circ$ grid and the other two coarser grids. These differences among the surface temperature from the $1/12^\circ$ grid with respect to that from the coarser grids is likely to be related to several factors. The first is the eddy component of the meridional heat transport, which can be significant in mesoscale eddy resolving models, while it is effectively zero in the coarser resolution cases. The second is the interaction of deep overflows with the surface flows via vortex stretching, near GIS ridges. The third is the difference of potential vorticity exerted by the significantly-different topographies on surface flows. Possibly, a combination of these factors plays a role in the difference. This

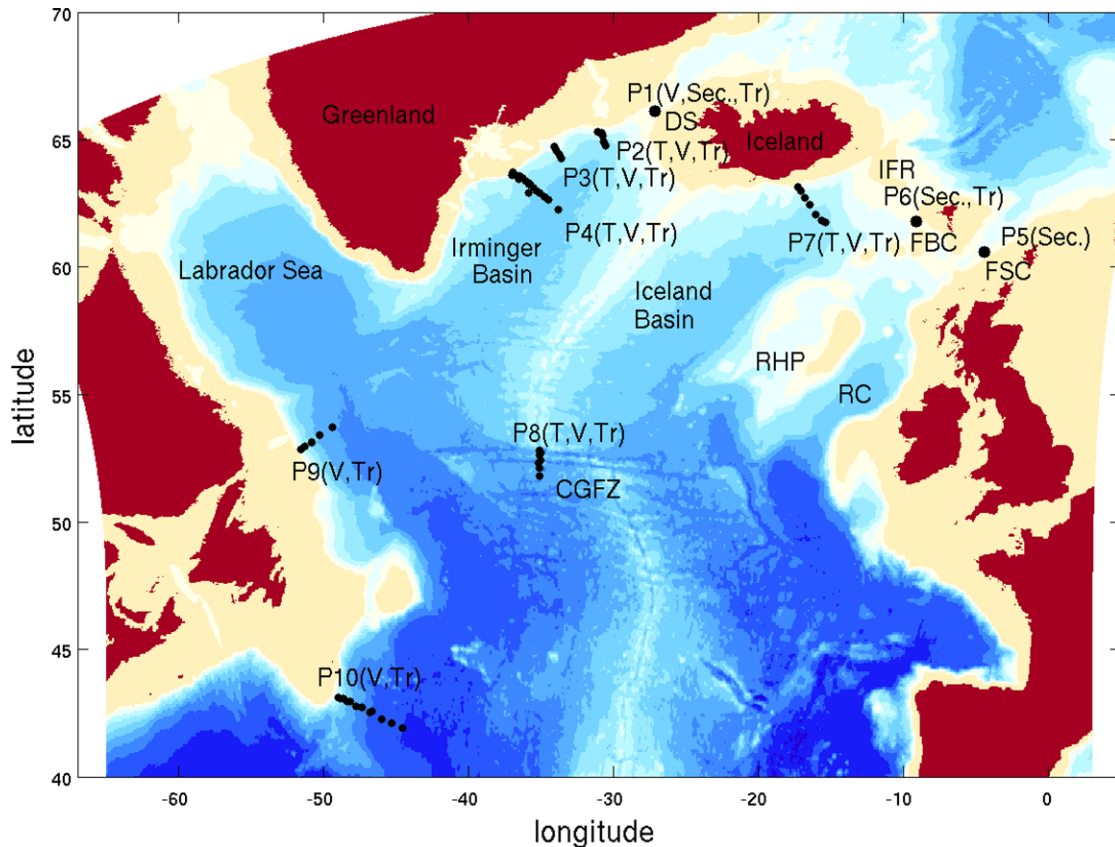


Fig. 8. Map of the ten experimental locations where the observational data are available. Black dots are the actual measuring points. The properties of available data are denoted at each location by 'V' = velocity profiles, 'T' = temperature profiles, 'Sec' = cross-sectional contours of density or temperature across the channel, and by 'Tr' = mass transport.

complex problem will be pursued in a future study, and here we focus only on the deep flows.

Location P7 in Fig. 8, southeast of Iceland, coincides with excessively strong flow across the Iceland-Faroe Ridge in the 1° simulations already discussed above. This finding is reinforced by Figs. 15 and 16a which show \bar{V} and T profiles from P7. The 1° flow speed is too large and the temperature is too low in the lowest 200 m above the bottom.

Observed and modeled flow speeds through the Charlie Gibbs fracture zone are small (Fig. 15b). All grids underestimate the flow. The 1° grid again suffers from a depth that is too shallow in the fairly narrow passage as a consequence of the smoothing and coarse grid resolution. The modeled temperature profiles are in good agreement with the observations (Fig. 16b).

The velocity field near the exit of the deep, cold flow from the Labrador Sea (P9 in Fig. 8) and east of the Grand Banks (P10) is spatially highly variable. Thus Fig. 17 depicts two profiles each of the mooring arrays, one from shallower depths and one from deeper depths. Success and failure of the simulations are mixed. The flow at the shallower site P9-1 in Fig. 17a is too fast in the $1/12^\circ$ grid, part of the apparently too vigorous circulation around the perimeter of the Labrador Sea at this resolution (see Fig. 7). None of the simulations capture the DWBC that appears in the observations at 2800 m depth at P9-2 (Fig. 17b). Only the $1/12^\circ$ simulation captures the DWBC at P10-1 (Fig. 17c).

4.2.3. Comparison of volume transport

One of the most important measures of validating our simulations is the volume transport of overflow waters. The vertical and horizontal integration inherent in the transports removes effects

of local spatial velocity variations such as those encountered in the context of Fig. 17 above. Observed estimates of the volume transport across the 10 sections P1–P10 introduced above and located in Fig. 8 are listed in Table 2 along with the corresponding model results. We have added four more sections to this list, P11–P14. P11 is to compare modeled transports at the southern tip of Greenland to that estimated by Dickson and Brown (1994). Observations are not yet available for the others in the eastern North Atlantic, but the model transports suggest that considerable amounts of overflow water might flow in these areas. Table 2 is accompanied by Fig. 18, which displays the transport numbers and direction in graphical form on a map of the North Atlantic. The volume transport, Q , is calculated from $Q = \int_A \bar{u} \cdot d\bar{A}$, where \bar{A} is the cross-sectional area vector pointing toward the overflow direction and \bar{u} is the velocity vector.

Table 2 and Fig. 18 demonstrate quantitatively that the $1/12^\circ$ -simulated volume transports match the moored observations quite well. Typical rms differences between observed and simulated Q are about 25%. In contrast, the $1/3^\circ$ and 1° simulations show both large under- and over-estimations at many locations. There seems to be no significant improvement in the model performance of reproducing overflow transports when the resolution is increased from 1° to $1/3^\circ$. The following provides detail.

The transports along P1–P4 in the Denmark Strait overflow shows an observed increase in Q owing to entrainment from 2.9 Sv at P1 to 10.7 Sv at P4 (Dickson and Brown, 1994). In the $1/12^\circ$ grid the entrainment rate is smaller; the simulated Q increases from 2.9 Sv to about 7 Sv.

As already indicated above, a combination of underestimated velocities (Fig. 13) and overestimated channel cross-section

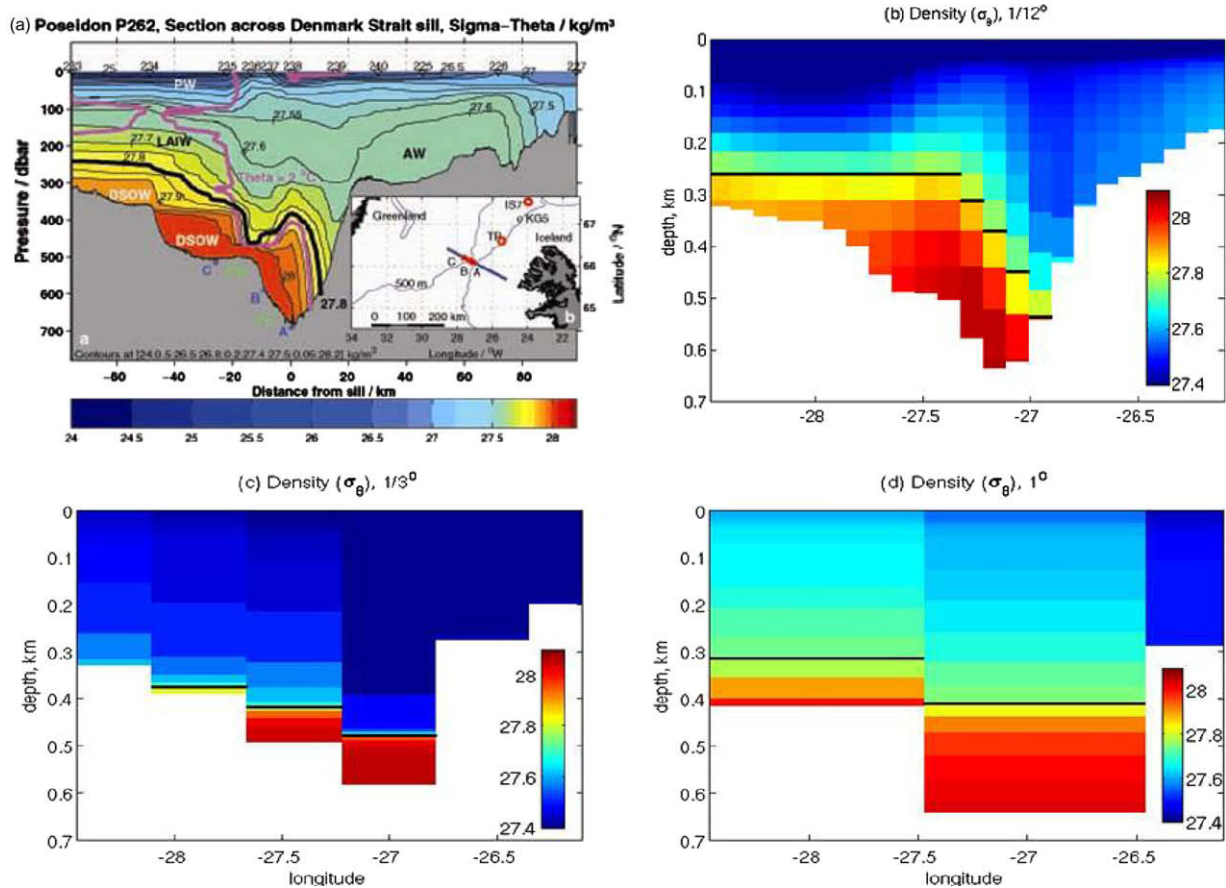


Fig. 9. Comparison of potential density sections across the sill of Denmark Strait at P1. (a) Observed σ_θ from Macrander et al. (2007). Simulations at (b) 1/12°, (c) 1/3°, and (d) 1° resolution. The heavy black line indicates the top of Denmark Strait Overflow Water.

(Fig. 9) leads to reasonable overflow transports in the 1° simulations in Denmark Strait. The fair match holds from P1 to P4. Transports from the 1/3° simulations are much too low at the sill of Denmark Strait and end up being an order of magnitude too small by P4. Above, we have diagnosed underestimates of both velocity (Fig. 13) and cross-section (Fig. 9) in the 1/3° grid. At the southern tip of Greenland (P11), the transport from the 1/12° case is in fair agreement with the observation. Similar values are obtained with 1°, but due to errors across the CGFZ compensating those over the Denmark Strait. Transport from the 1/3° grid is significantly lower, because subtropical pathways along the basin to east of the Mid Atlantic Ridge are followed in this case.

Observed transports are available at P6–P8 in the area from Scotland via Faroe Islands past southern Iceland to the Charlie Gibbs Fracture Zone. At these locations only the 1/12° simulations produce realistic transports. Transports in the 1/3° and 1° grids vary between large overestimates and large underestimates. For example, the 1° transport at P6, Faroe Bank Channel, is 0 Sv simply because there is no channel at this grid resolution (Fig. 11). The 1/3° transport is also far too small owing to poor resolution of the narrow channel. We already described excessive flow across the Iceland-Faroe Ridge in the 1° grid (Fig. 4b). This simulated flow continues westward and appears as overestimated transport at P7. In contrast, the 1/3° transport at P7 is too small owing to weak flow through the FBC and diversion of overflow water across the Wyville-Thompson Ridge (Fig. 4c).

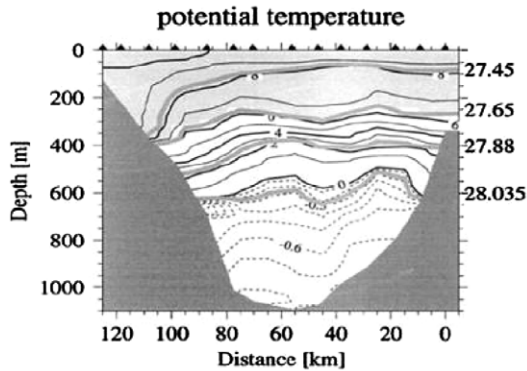
Problems with the 1° simulations continue at P8, the Charlie Gibbs Fracture Zone, where the transport is too large owing to excessive flow speeds (Fig. 15b) and excessive cross-section

(Fig. 6b), and with underestimated transports at P9 and P10, which lead into the Deep Western Boundary Current. Problems with the 1/3° simulations are no less severe, with underestimates at P8–P10.

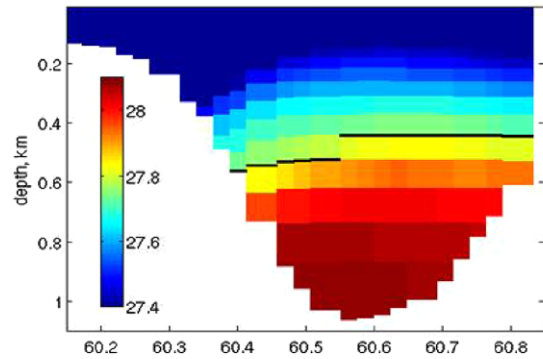
Overall, the 1/12° simulations agree with the observations at P8–P10 reasonably well, Q being significantly underestimated in the Charlie Gibbs Fracture Zone (P8) and at the southeastern corner of the Labrador Sea (P9). The latter location is interesting because some of the 1/12° velocities in the P9 section are overestimated (Fig. 17a), yet the transport proved to be underestimated.

The considerable realism of the 1/12° simulations encourages us to examine model transports at overflow density levels at locations where there are no transport observations. Specifically, we are interested in the deep flows along the east and west flanks of Rockall Plateau (sections P12 and P14 in Fig. 18). The latter is the southward continuation from the overflow across the Wyville-Thompson Ridge. Our interest also extend to the possible further continuation into the eastern basin of North Atlantic at section P14. Table 2 shows a 1/12° transport at overflow densities of 4.6 Sv. Such deep transports are significant within the deep ocean circulation. Fig. 18 suggests that these transports may be connected to the overflows in the area around the Faroe Islands even though it is not likely that all the deep transports at P12–P14 consist of overflow water. We expect them to be mixed with other water masses by both lateral and diapycnal processes. The question how much the deep circulation at overflow density levels east of the Mid Atlantic Ridge and south of Rockall Plateau is affected by the overflows in the Faroe region remains open.

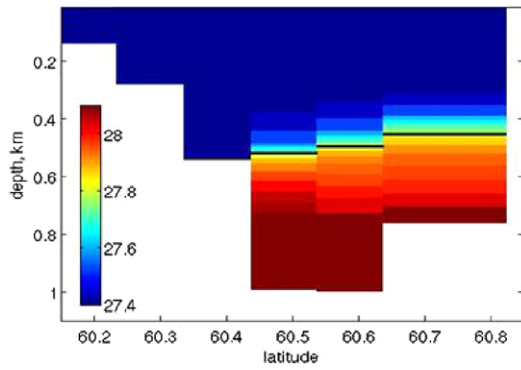
(a) Potential temp. distribution at FSC (Mauritzen et al., 2005).



(b) Density (σ_θ), 1/12 deg.



(c) Density (σ_θ), 1/3 deg.



(d) Density (σ_θ), 1.0 deg.

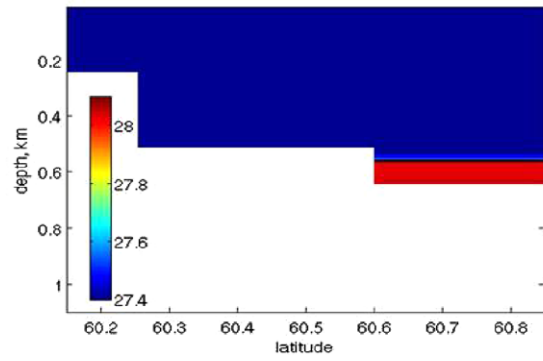
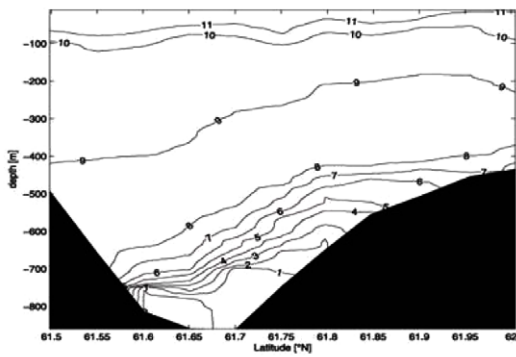
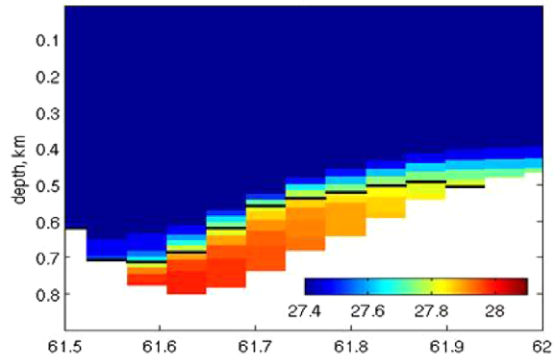


Fig. 10. Comparisons of hydrographic sections across Faroe Shetland Channel at P5. (a) Contour map of the observed potential temperature from Meincke (1974). (b) Simulated density contours from 1/12°, (c) 1/3°, and (d) 1°.

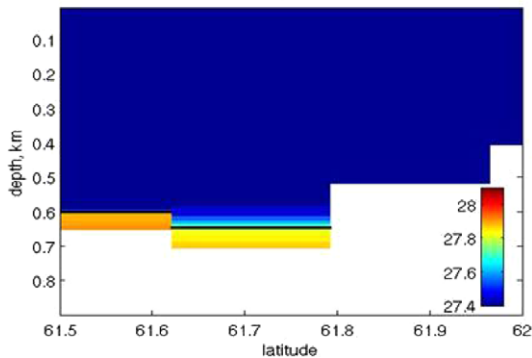
(a) Observed temp. distribution at FBC exit (Geyer et al., 2006).



(b) Density (σ_θ), 1/12 deg.



(c) Density (σ_θ), 1/3 deg.



(d) Density (σ_θ), 1.0 deg.

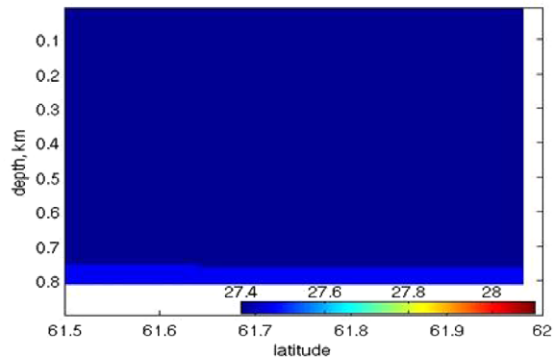


Fig. 11. Comparisons of hydrographic sections across the sill of Faroe Bank Channel at P6. (a) Contour map of the observed potential temperature from Geyer et al. (2006). (b) Simulated density contours from 1/12°, (c) 1/3°, and (d) 1°.

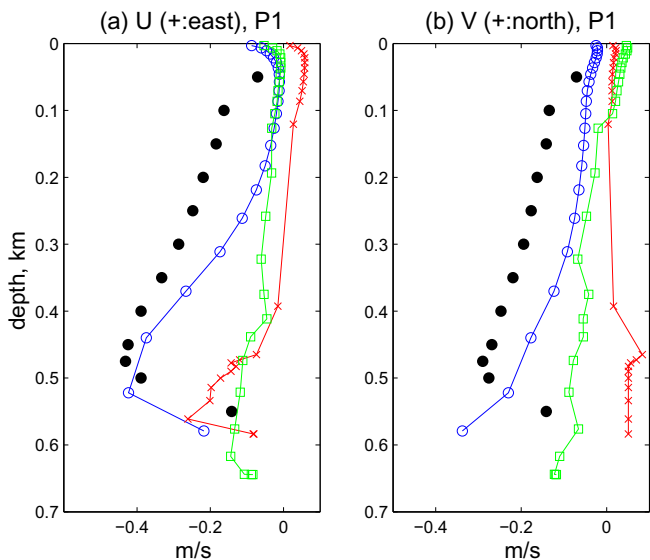


Fig. 12. Comparison of velocity profiles at P1 (see Fig. 8). (a) Eastward current component, (b) northward component. Black dots: observed data by Macrande et al. (2007); green squares: 1° simulation, red 'x' marks: $1/3^\circ$; and blue circles: $1/12^\circ$. (For interpretation of the references to colour in this figure legend, the reader is referred to the web version of this article.)

4.2.4. A simulation with hand-tuned topography

In light of the incorrect overflow pathways in coarse resolution simulations due to large errors in critical deep channels, we present an additional experiment in which the bathymetry is manually modified in an attempt to rectify the pathways. We present an experiment only with 1° since it contains less degrees of freedom regarding the number of grid points to be modified with respect to the $1/3^\circ$ case, but it can still serve to indicate the implications of taking this avenue.

The topographic hand tuning for the 1° case is focused at the FBC (P6), IFR (upstream of P7) and CGFZ (P8), which show the largest errors in this case (Table 2 and Fig. 18). The changes in the

topography are depicted in Fig. 19. In particular, we have manually created a one grid wide channel as a representation of FBC, since this was missing in the original grid. The depth of this channel is set to 780 m, which is a value that has been determined through several trials. The second topographic change is made at the IFR, which is unrealistically deep in the original version of the bathymetry. It is now replaced by the depths of neighboring grid points along the IFR. Finally, the lateral extent of the CGFZ is narrowed with respect to the original version in order to reduce the unrealistically high deep transport into the Irminger Basin. Since the hand tuning of topography is not based on any quantitative criteria, but on an iterative response of circulation, this is in fact a difficult inverse problem. As such, wide spread topographic manipulations can easily change the deep circulation significantly and obscure any understanding. Thus, we limit these changes to these three regions in order to minimize the hand-tuned area.

The results of the topographic manipulations are shown in Fig. 20 and Table 2. We immediately see that near locations of topographic changes, namely at P6 (FBC), P7 (downstream of IFR) and P8 (CGFZ), the results have improved significantly. The reduction of transport across CGFZ has also increased the southward flow along the eastern flank of the MAR (for which we do not have observations). Nevertheless, the reduced westward transport through CGFZ appears to have deteriorated the results in the Irminger Basin. This is because in the previous version of the 1° topography, the unrealistically high transport across CGFZ was compensating for errors in the DSO (this is a case of two errors correcting the final result). In the modified bathymetry, errors in the dynamics of DSO are more apparent. Even though the difference is not very significant, it indicates a need for further topographic adjustments in the vicinity of the Denmark Strait in order to further improve the results. Finally, we see far reduced transports at P10, which seems to be an indication of the sensitivity of the circulation near the Grand Banks (possibly a complex bifurcation region) to any upstream changes, as emphasized by Bower et al. (2008).

The new results from the modified topography seem to give the following messages. First, the hand-tuning of the topography in a coarse resolution model may lead to better results in some areas,

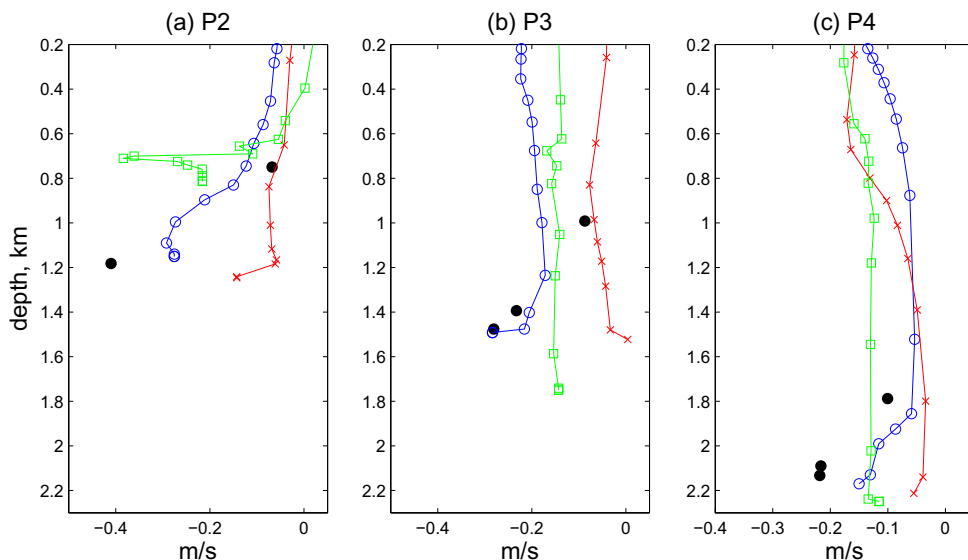


Fig. 13. Comparison of velocity profiles from sections at (a) P2, (b) P3 and (c) P4; \bar{V} velocity component positive northeast. Black dots: observed data by Dickson and Brown (1994); simulations, green squares: 1° , red 'x' marks: $1/3^\circ$, and blue circles: $1/12^\circ$. The velocity profiles shown are from near the shoreward ends of the mooring arrays (P2: 65.222°N , 30.848°W ; P3: 65.550°N , 33.927°W ; P4: 63.383°N , 36.088°W). (For interpretation of the references to colour in this figure legend, the reader is referred to the web version of this article.)

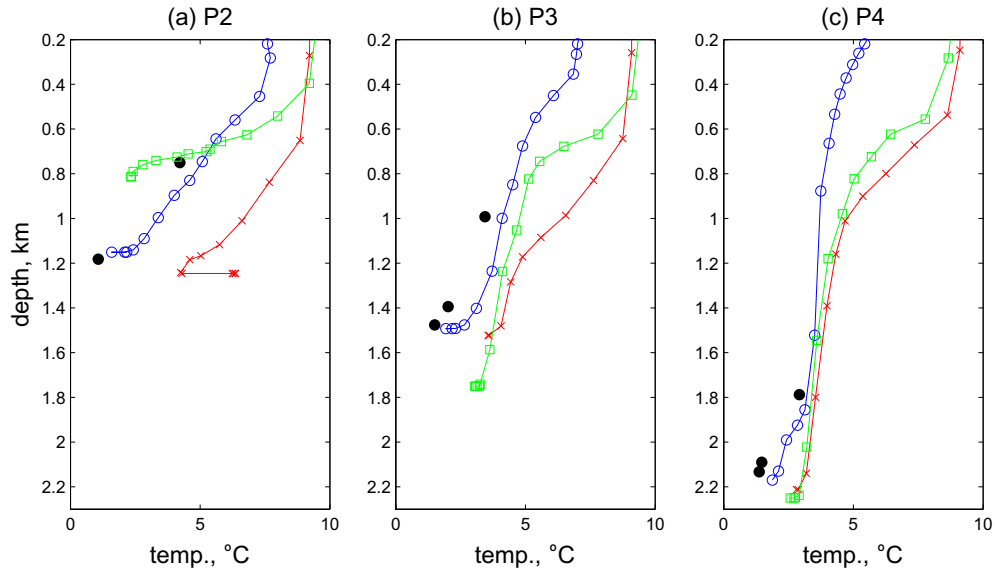


Fig. 14. Comparison of temperature profiles at (a) P2, (b) P3 and (c) P4. The data source and the notation are those of Fig. 13.

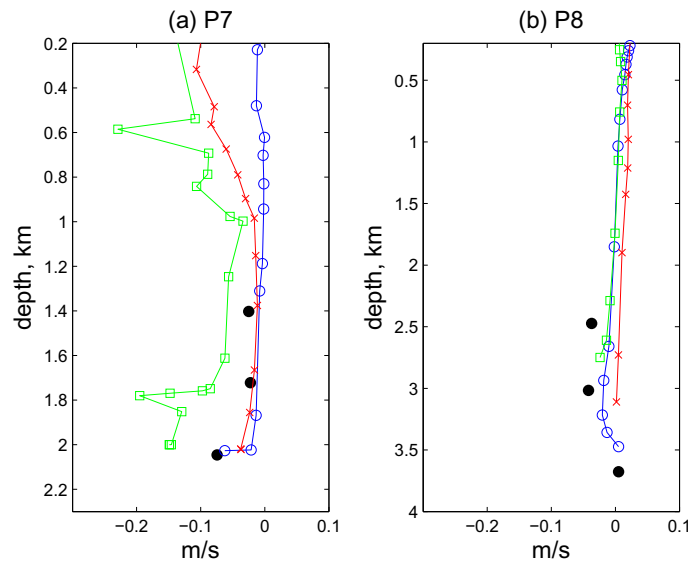


Fig. 15. Comparison of velocity profiles at (a) P7, and (b) P8; \bar{V} , positive northeast for P7 and ordinary V for P8. Black dots: observed data from Schmitz (1996) for P7 and Saunders (1996) for P8; simulations, green squares: 1° , red 'x' marks: $1/3^\circ$, and blue circles: $1/12^\circ$. P7: mooring at 62.444°N , 16.471°W ; P8: 52.688°N , 35.070°W . (For interpretation of the references to colour in this figure legend, the reader is referred to the web version of this article.)

but it may disturb the accuracy of results at some other locations as well. It is a complex inverse problem that has the prospect of becoming more difficult when the nonlinearities in the flow increase (e.g., in eddy-permitting cases). Second, it can only be attempted if the circulation details are known on the basis of the existing observations. Sparse data, highly-variable flows and rapidly-changing forcing conditions (all of which possibly apply in the Nordic Seas presently) can lead to misleading results. Subsequently, it is not clear how to develop quantitative techniques to go about this approach systematically.

5. Summary and discussion

Pathways of overflows across the Greenland–Iceland–Scotland ridge system are investigated using a community ocean circulation model (HYCOM) at three different horizontal grid resolutions of 1° ,

$1/3^\circ$ and $1/12^\circ$. Initial conditions and surface forcing are nearly identical in all cases. We focus on the effect of differences in the model seafloor topography at the different resolutions. The model seafloor topographies are generated using standard interpolation routines. The simulations are evaluated qualitatively and quantitatively by comparing them with observations, hydrographic sections and moored current and temperature measurements.

We find that the mean structure of the overflows in Denmark Strait and Faroe Bank Channel are simulated only at the highest resolution employed, $1/12^\circ$. Simulations of lower resolution fail quantitatively or even qualitatively. The 1° grid, for example, simply does not have a Faroe Bank Channel and thus no overflow through it. Severe problems with the lower resolution cases extend far beyond the actual overflows to large parts of the deep circulation at overflow density levels. In the lower resolution simulations part of the overflow waters enter the wrong basins of the ocean, for

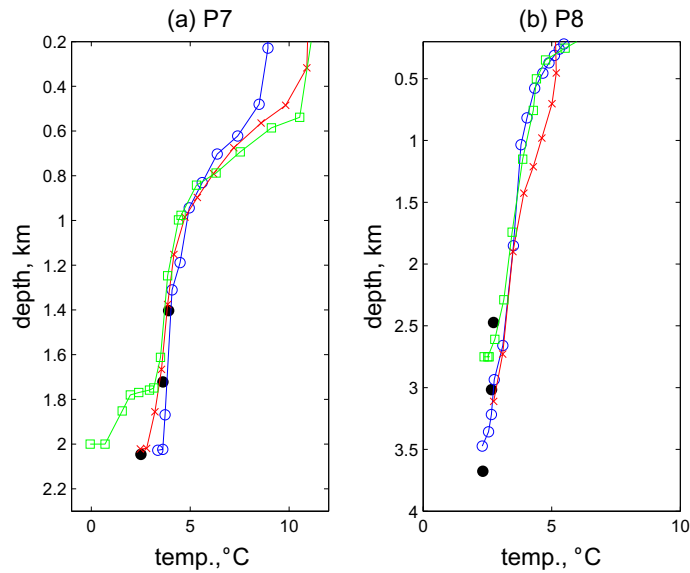


Fig. 16. Comparison of temperature profiles (a) P7, and (b) P8. Data sources and notation follow Fig. 15.

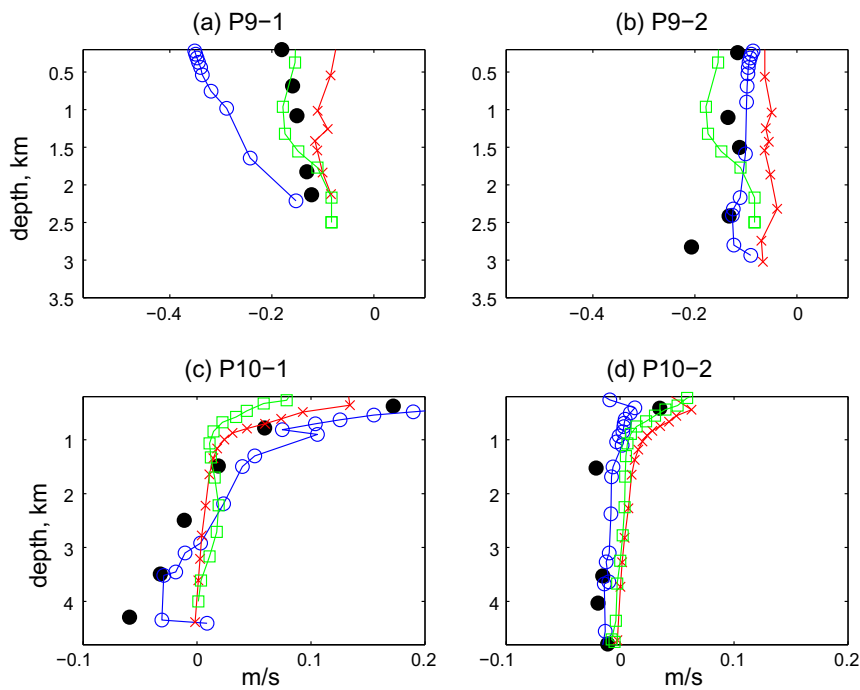


Fig. 17. Comparison of velocity profiles from (a and b) the southern Labrador Sea (P9 in Fig. 8) and (c and d) southeast of the Grand Banks (P10). The rotated velocity component depicted is positive northwestward for P9 and positive northeastward for P10. Black dots: observed data by Fischer et al. (2004) for P9 and Sherwin and Turrell (2005) for P10; simulations, green squares: 1° , red 'x' marks: $1/3^\circ$, and blue circles: $1/12^\circ$. P9-1: mooring at 52.958°N , 51.300°W ; P9-2: 53.141°N , 50.866°W ; P10-1: 42.566°N , 46.686°W ; P10-2: 41.907°N , 44.575°W . (For interpretation of the references to colour in this figure legend, the reader is referred to the web version of this article.)

example, in the $1/3^\circ$ case, into Rockall Basin instead of west into Iceland Basin. Conversely, the $1/12^\circ$ simulations compare favorably, although not perfectly, with observations far from the overflow locations in the Charlie Gibbs Fracture Zone, Labrador Sea and to a degree even in the Deep Western Boundary Current off the Grand Banks.

This study was conceived with the notion that realistic climate models, and especially climate change models, need to have a realistic deep ocean circulation. The connection between the deep ocean and the surface that affects the atmosphere, and hence climate, is the vertical overturning in the ocean, in our case the

Atlantic Meridional Overturning Circulation. Herein, we asked the question of what grid resolution is required in isopycnic coordinate models to produce fairly realistic overflow pathways and AMOC, in the absence of any specific treatment of overflows. Our answer is that the resolution needs to be an order of magnitude larger than the typical 1° of current climate models. This resolution is mainly dictated by the main pathways of the sea floor. Both 1° and $1/3^\circ$ simulations show both large under- and overestimations at many locations. There seems to be no significant improvement in the model performance of reproducing overflow transports when the resolution is increased from 1° to $1/3^\circ$. This

Table 2
Observed and simulated volume transports. Error is calculated from $Q_{model}/Q_{observed} - 1$.

	Observed.	1/12°(error%)	1/3°(error%)	1°(error%)	modified 1°(error%)
P1	2.9 Sv	2.93 Sv (1)	0.75 Sv (-74)	1.79 Sv (-38)	1.58Sv (-46)
P2	5.2 Sv	4.33 Sv (-17)	0.74 Sv (-86)	3.86 Sv (-26)	2.04 Sv (-61)
P3	5.1 Sv	5.93 Sv (16)	1.39 Sv (-73)	5.85 Sv (15)	5.34 Sv (5)
P4	10.7 Sv	6.94 Sv (-35)	1.49 Sv (-86)	8.41 Sv (-21)	6.49 Sv (-39)
P5	-	2.96 Sv	4.01 Sv	0.34 Sv	1.80 Sv
P6	1.9 Sv	2.20 Sv (16)	0.38 Sv (-80)	0.0 Sv (-100)	2.20 Sv (16)
P7	3.2 Sv	2.79 Sv (-13)	1.66 Sv (-48)	5.42 Sv (69)	3.43 Sv (7)
P8	2.4 Sv	1.31 Sv (-45)	0.17 Sv (-93)	7.11 Sv (196)	1.44 Sv (-40)
P9	17 Sv	10.85 Sv (-36)	6.85 Sv (-60)	9.15 Sv (-46)	9.51 Sv (-44)
P10	12 Sv	11.55 Sv (-4)	3.18 Sv (-74)	4.66 Sv (-61)	1.73 Sv (-86)
P11	13.3 Sv	9.44 Sv (-29)	3.32 Sv (-75)	8.76 Sv (-34)	7.49 Sv (-44)
P12	-	1.51 Sv	1.29 Sv	2.58 Sv	1.69 Sv
P13	-	2.23 Sv	6.30 Sv	0.78 Sv	1.89 Sv
P14	-	4.60 Sv	7.07 Sv	2.92 Sv	4.32 Sv

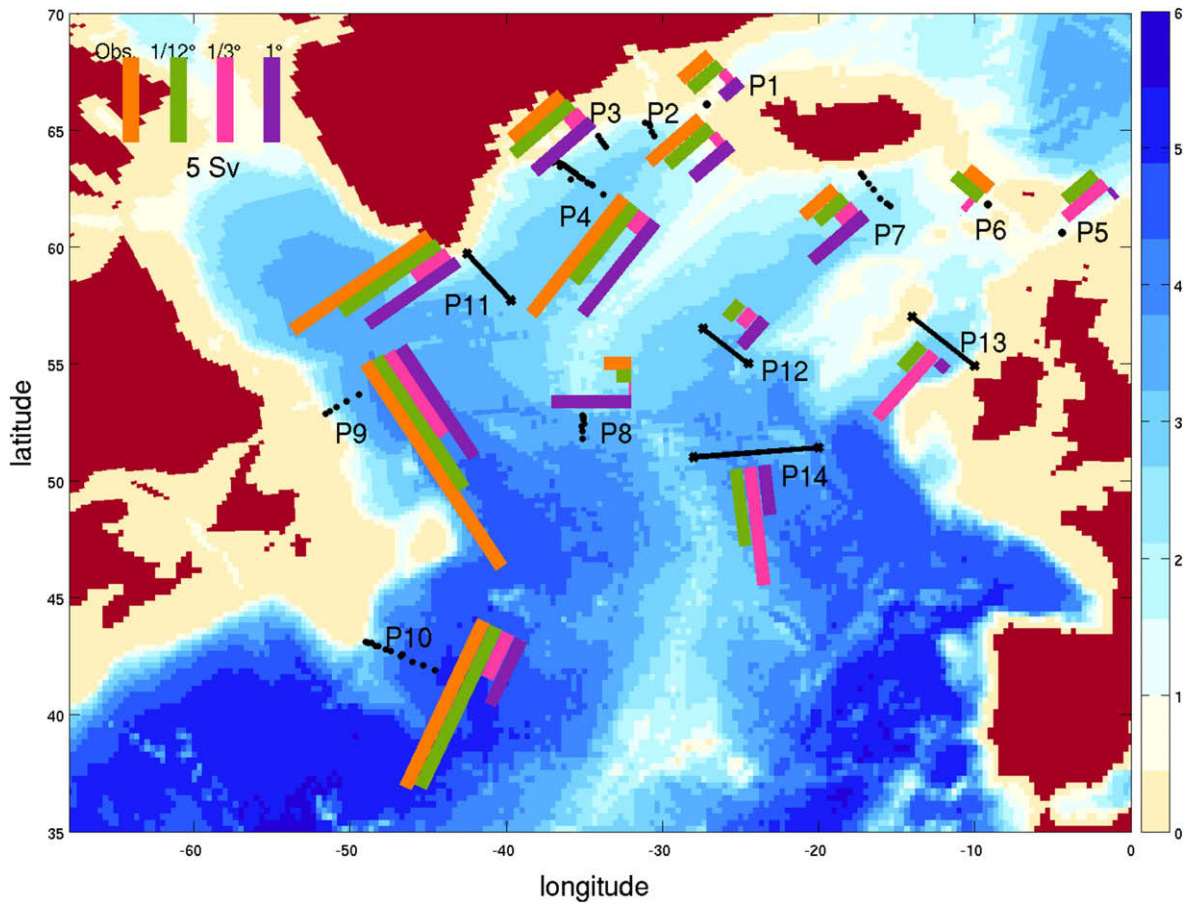


Fig. 18. Map of overflow water volume transports showing comparison between the observed and modeled Q at each of the sections P1–P11. The bars are directed into the mean overflow direction at each location. Orange bars: observation; green bars: 1/12°; pink bars: 1/3°; purple bars: 1°. Observations are unavailable for sections P12–P14. (For interpretation of the references to colour in this figure legend, the reader is referred to the web version of this article.)

implies that under-resolved topography sets a threshold as to prohibit the usual gradual improvement in model performance until dynamically important channels are adequately represented in the model domain.

In order to improve the deep circulation resulting from large topographic errors, manual corrections are made to IFR, FBC and CGFZ in an experiment with 1° horizontal resolution. The results show significant reductions in errors near these regions, but simultaneously creation of somewhat higher errors than before in other parts of the basin as well. We conclude that such manual corrections to bathymetry could be useful provided that they are limited

to the most obvious locations, such as blocked or significantly-overestimated channels.

Alternatives to our approach of explicit simulations of overflows, namely MSBC-type parameterizations of overflows, and depth- or sigma coordinates are beyond the scope of this paper. While the MSBC is shown to result in excellent agreement with high-resolution model output for the Mediterranean Sea overflow (Xu et al., 2007), it is not clear how to extend its applicability to overflows across the Iceland–Scotland ridge and further downstream. High-resolution simulations by Riemenschneider and Legg (2007) show patterns far more complex than those captured with

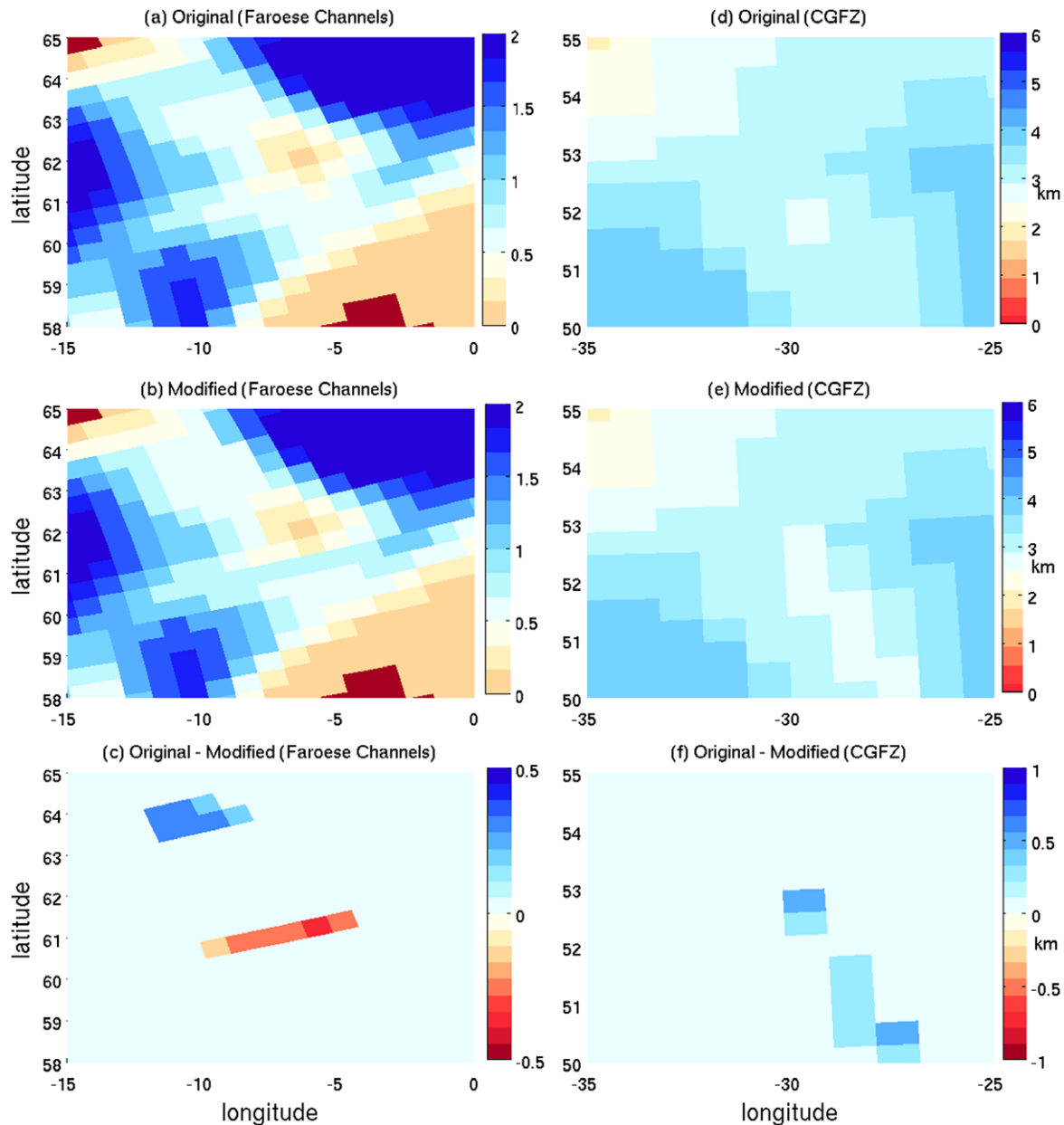


Fig. 19. Summary of the topographic changes introduced in a new 1° model run. (a) The original topography, (b) modified topography, (c) the difference (original-modified) of topography near the Farøese channels. (d–f) The same for the region near the CGFZ. The depth color scale is in km. (For interpretation of the references to colour in this figure legend, the reader is referred to the web version of this article.)

$1/12^\circ$ HYCOM for the FBC overflow. Existence of complex hydraulic phenomena with possible impacts on mixing have also been put forth by Pratt et al. (2007). Clearly, we have discussed requirements to capture only the very basic mean overflow pathways here, and more comprehensive investigations of the fluid dynamical problems must await even higher resolution computations of the general circulation.

On a technical note, this paper indicates that great care needs to be taken in generating model seafloor topographies, especially at lower resolutions. The common smoothing applied in the topography-generating algorithms can cause undesirable and unrealistic leakages of deeper into shallower depths. In our case this leads to a non-existing passage across the Iceland-Farøe Ridge at 1° resolution. As such, topography-generating algorithms may have to be reexamined to develop techniques that help preserve the main pathways as accurately as possible on coarse meshes. Perhaps a

contribution of this study would be to increase the awareness in the modeling community of the sensitivity of the deep circulation to details in preprocessing of bathymetry and foster future studies on improved interpolation methods.

Acknowledgement

We gratefully acknowledge the support of the National Science Foundation for the Climate Process Team on Gravity Current Entrainment (CPT-GCE; grant OCE 0336799 and 0611579). Z. Garraffo's participation was funded through University of Miami's Center for Computational Science. We benefited greatly from discussions with our colleagues in the CPT-GCE. In particular, we would like to thank Jim Price for providing excellent guidance during early stages of this study. Cecilie Mauritzen, Florian Geyer and Andreas Macrander kindly gave their permission to use figures

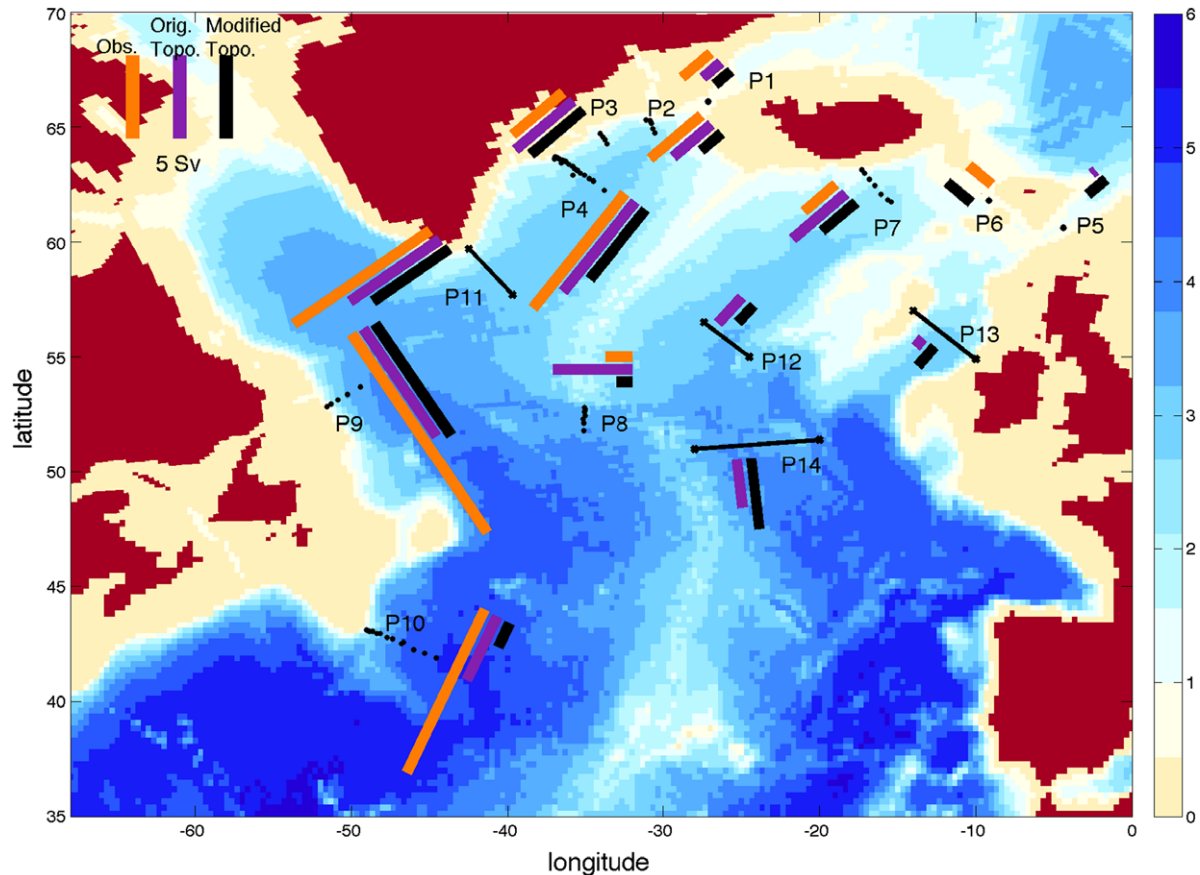


Fig. 20. Map of overflow water volume transports showing comparison between the 1° model runs with topographic changes. The sections are same in Fig. 18. Orange bars: observation; green bars: 1° original topography; pink bars: 1° modified topography. (For interpretation of the references to colour in this figure legend, the reader is referred to the web version of this article.)

from their papers. We thank A. Wallcraft of the Naval Research Lab for assistance in HYCOM issues. We appreciate the constructive comments of two anonymous reviewers and editor Stephen Griffies which led to a significant improvement of the manuscript and the experiment presented in Section 4.2.4.

References

- Beismann, J.O., Barnier, B., 2004. Variability of the meridional overturning circulation of the North Atlantic: sensitivity to overflows of dense water masses. *Ocean Dynamics* 54, 92–106.
- Bentsen, M., Drange, H., Furevik, T., Zhou, T., 2004. Simulated variability of the Atlantic meridional overturning circulation. *Climate Dynamics* 22, 701–720.
- Bleck, R., 2002. An oceanic general circulation model framed in hybrid isopycnic-Cartesian coordinates. *Ocean Modelling* 4, 55–88.
- Blindheim, J., Francisco, R., 2004. Water-mass formation and distribution in the Nordic Seas during the 1990s. *ICES Journal of Marine Science* 61, 846–863.
- Bower, A., Lozier, M.S., Gary, S.F., Böning, C.W., submitted for publication. Interior pathways of the North Atlantic Meridional Overturning Circulation. *Nature*.
- Broecker, W.S., 2003. Does the trigger for abrupt climate change reside in the ocean or in the atmosphere? *Science* 300, 1519–1522.
- Bryden, H.L., Longworth, H.R., Cunningham, S.A., 2005. Slowing of the Atlantic meridional overturning circulation at 25°N. *Nature* 438, 655–657.
- Chang, Y.S., Özgökmen, T., Peters, H., Xu, X., 2008. Numerical simulation of Red Sea outflow using HYCOM and comparison with REDSOX observations. *J. Phys. Oceanogr.* 38 (2), 337–358.
- Chang, Y.S., Xu, X., Özgökmen, T.M., Chassignet, E.P., Peters, H., Fischer, P., 2005. Comparison of gravity current mixing parameterizations and calibration using a high-resolution 3D nonhydrostatic spectral element model. *Ocean Modelling* 10, 342–368.
- Chassignet, E.P., Hurlburt, H.E., Smedstad, O.M., Halliwell, G.R., Hogan, P.J., Wallcraft, A.J., Baraille, R., Bleck, R., 2007. The HYCOM (HYbrid Coordinate Ocean Model) data assimilative system. *J. Mar. Sys.* 65, 60–83.
- Chassignet, E.P., Smith, L.T., Halliwell, G.R., Bleck, R., 2003. North Atlantic simulation with the HYbrid Coordinate Ocean Model (HYCOM): impact of the vertical coordinate choice, reference density, and thermobaricity. *J. Phys. Oceanogr.* 33, 2504–2526.
- Cunningham, S.A., Kanzow, T., Rayner, D., Baringer, M., Johns, W.E., Marotzke, J., Longworth, H.R., Grant, E.M., Hirschi, J., Beal, L.M., Meinen, C.S., Bryden, H.L., 2007. Temporal variability of the Atlantic meridional overturning circulation at 265°N. *Science* 317, 935–938.
- Dickson, R.R., Brown, J., 1994. The production of North Atlantic deep water: sources, rates, and pathways. *J. Geophys. Res.* 99 (C6), 12319–12341.
- Ellett, D.J., Roberts, D.G., 1973. The overflow of Norwegian sea deep water across the Wyville-Thomson ridge. *Deep Sea Res.* 20, 819–835.
- Fischer, J., Schott, F.A., Dengler, M., 2004. Boundary circulation at the exit of the Labrador sea. *J. Phys. Oceanogr.* 34, 1548–1570.
- Garraffo, Z.D., Mariano, A.J., Griffa, A., Veneziani, C., Chassignet, E.P., 2001. Lagrangian data in a high resolution numerical simulation of the North Atlantic. I. Comparison with in-situ drifter data. *J. Mar. Sys.* 29, 157–176.
- Geyer, F., Østerhus, S., Hansen, B., Quadfasel, D., 2006. Observations of highly regular oscillations in the overflow plume downstream of the Faroe Bank Channel. *J. Geophys. Res.* 111 (C12020). doi:10.1029/2006JC003693.
- Girton, J.B., Sanford, T.B., Käse, R.F., 2001. Synoptic sections of the Denmark strait overflow. *Geophys. Res. Lett.* 28 (8), 1619–1622.
- Gnanadesikan, A., Dixon, K., Griffies, S., Balaji, V., Barreiro, M., Beesley, J., Cooke, W., Delworth, T., Gerdes, R., Harrison, M., Held, I., Hurlin, W., Lee, H., Liang, Z., Nong, G., Pacanowski, R., Rosati, A., Russel, J., Samuels, B., Song, Q., Spelman, M., Stouffer, R., Sweeney, C., Vecchi, G., Winton, M., Wittenberg, A., Zeng, F., Zhang, R., Dunne, J., 2006. GFDL's CM2 global coupled climate models. Part II. The baseline ocean simulation. *J. Climate* 6, 675–697.
- Gregory, J.M., Dixon, K.W., Stouffer, R.J., Weaver, A.J., Driesschaert, E., Eby, M., Fichefet, T., Hasumi, H., Hu, A., Jungclaus, J.H., Kamenkovich, I.V., Levermann, A., Montoya, M., Murakami, S., Nawrath, S., Oka, A., Sokolov, A.P., Thorpe, R.B., 2005. A model intercomparison of changes in the Atlantic thermohaline circulation in response to increasing atmospheric CO₂ concentration. *Geophys. Res. Lett.* 32 (L12703). doi:10.1029/2005GL023209.
- Häkkinen, S., Rhines, P.B., 2004. Decline of subpolar North Atlantic circulation during 1990s. *Science* 304, 555–559.
- Halliwell, G.R., 2004. Evaluation of vertical coordinate and vertical mixing algorithms in the HYbrid-Coordinate Ocean Model (HYCOM). *Ocean Modelling* 7, 285–322.

- Hansen, B., Østerhus, S., 2000. North Atlantic-nordic seas exchanges. *Prog. Oceanogr.* 45, 109–208.
- Hansen, B., Østerhus, S., Quadfasel, D., Turrell, W., 2004. Already the day after tomorrow? *Science* 305, 953–954.
- Kanzow, T., Cunningham, S.A., Rayner, D., Hirschi, J., Johns, W.E., Baringer, M.O., Bryden, H.L., Beal, L.M., Meinen, C.S., Marotzke, J., 2007. Observed flow compensation associated with the MOC at 26.5°N in the Atlantic. *Science* 317, 938–941.
- Knudsen, 1898. Den Danske Ingolf-expedition. Bianco Lunos Kgl Hof-Bogtrykkeri (F. Dreyer). København, 1 (2), 21–154.
- Lake, I., Lundberg, P., 2006. Seasonal barotropic modulation of the deep-water overflow through the Faroe Bank Channel. *J. Phys. Oceanogr.* 36, 2328–2339.
- Large, W.G., McWilliams, J.C., Doney, S.C., 1994. Oceanic vertical mixing: a review and a model with a nonlocal boundary layer parameterization. *Rev. Geophys.* 32, 363–403.
- Legg, S., Chang, Y., Chassignet, E., Danabasoglu, G., Ezer, T., Gordon, A., Griffies, S., Hallberg, R., Jackson, L., Large, W., Ozgokmen, T., Peters, H., Price, J., Riemenschneider, U., Wu, W., Xu, X., Yang, J., in press. Improving Oceanic Overflow Representation in Climate Models: The Gravity Current Entrainment Climate Process Team. *Bull. Am. Met. Soc.*
- Levitus, S., Burgett, R., Boyer, T.P., 1994. World Ocean Atlas 1994, vol. 3. Salinity NOAA Atlas NESDIS 3, US Department of Commerce, Washington, DC, p. 99.
- Levitus, S., Boyer, T.P., 1994. World Ocean Atlas 1994 Volume 4: Temperature. NOAA Atlas NESDIS 4, US Department of Commerce, Washington, DC, 117p.
- Lumpkin, R., Speer, K., 2007. Notes and correspondence: global ocean meridional overturning. *J. Phys. Oceanogr.* 37, 2550–2562.
- Macrandrer, A., Käse, R.H., Send, U., Valdimarsson, H., Jonsson, S., 2007. Spatial and temporal structure of the Denmark Strait Overflow revealed by acoustic observations. *Ocean Dynamics* 57, 75–89.
- Mauritzen, C., Price, J., Sanford, T., Torres, D., 2005. Circulation and mixing in the Faroese Channels. *Deep Sea. Res.* 52, 883–913.
- Meincke, J., 1974. Overflow'73 – large-scale features of the overflow across the Iceland-Faroe Ridge. *ICES CM 1974/C*, 7, p. 10.
- Price, J.F., Yang, J., 1998. Marginal sea overflow for climate simulations. In: Chassignet, E.P., Verron, J. (Eds.), *Ocean Modelling and Parameterizations*. Kluwer Academic Publishers, New York, pp. 155–170.
- Quadfasel, D., 2005. The Atlantic heat conveyor slows. *Nature* 438, 565–566.
- Pratt, L.J., Riemenschneider, U., Helfrich, K.R., 2007. A transverse hydraulic jump in a model of the Faroe Bank Channel outflow. *Ocean Modelling* 19, 1–9.
- Riemenschneider, U., Legg, S., 2007. Regional simulations of the Faroe Bank Channel overflow in a level model. *Ocean Modelling* 17, 93–122.
- Roberts, M.J., Wood, R.A., 1997. Topographic sensitivity studies with a Bryan-Cox-Type Ocean Model. *J. Phys. Oceanogr.* 27, 823–836.
- Saunders, P.M., 1994. The flux of overflow water through the Charlie–Gibbs Fracture Zone. *J. Geophys. Res.* 99 (C6), 12343–12355.
- Saunders, P.M., 1996. The flux of dense cold overflow water southeast of Iceland. *J. Phys. Oceanogr.* 26, 85–95.
- Schmitz, W.J., 1996. On the World Ocean Circulation: Volume I. WHOI-96-03 Technical Report, 141p.
- Sherwin, T.J., Turrell, W.R., 2005. Mixing and advection of a cold water cascade over the Wyville–Thomson Ridge. *Deep Sea. Res.* 52, 1392–1413.
- Steele, J.H., 1961. Notes on the deep water overflows across the Iceland-Faroe Ridge. *Rapports et Proces-Verbaux des Reunions du Conseil International pour l'Exploration de la Mer*, 149, 469–473.
- Steele, J.H., 1967. Current measurements on the Iceland-Faroe Ridge. *Deep Sea Res.* 14, 469–473.
- Swift, J.H., 1984. The circulation of the Denmark Strait and Iceland-Scotland overflow waters in the North Atlantic. *Deep Sea Res.* 31, 1339–1355.
- Tait, J.B., 1967. The Iceland-Faroe Ridge international (ICES)'Overflow' expedition, May-June 1960. *Rapports et Proces-Verbaux des Reunions du Conseil International pour l'Exploration de la Mer*, 157, 38–149.
- Teague, W.J., Carron, M.J., Hogan, P.J., 1990. A comparison between the generalized digital environmental model and Levitus climatologies. *J. Geophys. Res.* 95 (C5), 7167–7183.
- Uppala, S.M., and the ERA-40 Group, 2005: The ERA-40 re-analysis. *Q.J.R. Meteorol. Soc.* 131, 2961–3012. doi:10.1256/qj.04.176.
- van Aken, H.M., 1998. Current measurement in the Iceland Basin. *ICES Cooperative Research Report* 225, 215–227.
- Weaver, A.J., Bitz, C.M., Fanning, A.F., Holland, M.M., 1999. Thermohaline circulation: high-latitude phenomena and the difference between Pacific and Atlantic. *Annu. Rev. Earth Planet. Sci.* 27, 231–285.
- Wu, W., Danabasoglu, G., Large, W.G., 2007. On the effects of the parameterized Mediterranean overflow on North Atlantic ocean circulation and climate. *Ocean Modelling*, 19, 31–52.
- Wunsch, C., Heimbach, P., 2006. Estimated decadal changes in the North Atlantic Meridional Overturning Circulation and heat flux 1993–2004. *J. Phys. Oceanogr.* 36, 2012–2024.
- Xu, X., Chang, Y.S., Peters, H., Özgökmen, T.M., Chassignet, E.P., 2006. Parameterization of gravity current entrainment for ocean circulation models using a high-order 3D nonhydrostatic spectral element model. *Ocean Modelling* 14, 19–44.
- Xu, X., Chassignet, E.P., Price, J.F., Özgökmen, T.M., Peters, H., 2007. A regional modeling study of the entraining Mediterranean outflow. *J. Geophys. Res.* Oceans 112, C12005. doi:10.1029/2007JC004145.